ACS APPLIED MATERIALS & INTERFACES

Research Article

Cite This: ACS Appl. Mater. Interfaces 2018, 10, 26678−26686

www.acsami.org

Enhancing Gas Sorption and Separation Performance via Bisbenzimidazole Functionalization of Highly Porous Covalent Triazine Frameworks

Jianfeng Du,[†] Yuchuan Liu,[†] Rajamani Krishna,[‡] Yue Yu,[†] Yuanzheng Cui,[†] Shun Wang,[†] Yunling Liu,[†] Xiaowei Song,*[,†] and Zhiqiang Liang*[,†]

[†]State Key Laboratory of Inorganic Synthesis and Preparative Chemistry, Jilin University, Changchun 130012, P. R. China

[‡]Van't Hoff Institute for Molecular Sciences, University of Amsterdam, Science Park 904, 1098 XH Amsterdam, The Netherlands

Supporting Information

ABSTRACT: In this paper, a series of bisbenzimidazole-functionalized highly porous covalent triazine frameworks (**CTF-BIBs**) has been constructed from a new organic building block, 1,4-bis(5-cyano-1*H*-benzimidazole-2-yl)benzene, via ionothermal polymerization. The physical porosity and gas adsorption properties of these **CTF-BIBs** were characterized, and the resulting **CTF-BIBs** exhibit significantly high Brunauer−Emmett−Teller surface areas (1636−2088 $m^2\ g^{-1}$) and notable CO_2 uptakes (86.4−97.6 $cm^3\ g^{-1}$ at 273 K and 1 bar; 48.5−56.8 $cm^3\ g^{-1}$ at 298 K and 1 bar). More importantly, these **CTF-BIBs** exhibit excellent selective separation abilities for CO_2/N_2, CO_2/CH_4, C_2H_6/CH_4, and C_3H_8/CH_4, particularly for equimolar mixtures C_3H_8/CH_4 (386.6 for **CTF-BIB-1** under 1 bar and 298 K). Furthermore, transient breakthrough simulations were carried out for equimolar $CO_2/C_3H_8/C_2H_6/CH_4$ mixtures, and **CTF-BIBs** display good separation performance in industrial fixed bed adsorbers. These results clearly demonstrate that the synthesized **CTF-BIBs** may serve as potential materials for CO_2 capture and adsorptive separation for small hydrocarbons.

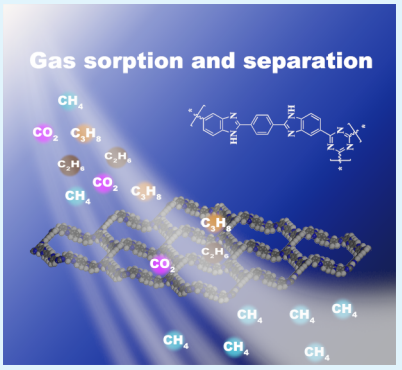

KEYWORDS: *covalent triazine frameworks, benzimidazole, CO_2 capture, small hydrocarbons, gas separation*

INTRODUCTION

Worldwide environment and energy issues have attracted enormous attention because of global warming and diminishing fossil fuel reserves. CO_2 capture and storage (CCS) technologies are considered as a vital proposal to solve the greenhouse effects caused by the escalating level of anthropogenic CO_2.[1] The traditional CCS technologies, including amine scrubbing and cryogenic separation, suffer high cost, severe corrosion of equipment, and chemical decomposition in the regeneration process.[2,3] Hence, developing new methods and materials for CCS is an urgent task to alleviate or eliminate the abovementioned constraints. In recent years, porous adsorbents have demonstrated significant promise for CCS.[4−6]

Currently, natural gas mainly consisting of methane (CH_4) has become a major energy fuel instead of controversial coal and oil, which is attributed to the lowest carbon amount of CH_4 and the least CO_2 emission per unit energy.[7,8] However, varying amounts of impurities in natural gas, such as CO_2, C_2H_6, C_3H_8, and so forth, will severely reduce the utilization efficiency of CH_4. Thus, the selective separation of CO_2/CH_4, C_2H_6/CH_4, and C_3H_8/CH_4 is of immense importance for purifying natural gas.[9−12] The cryogenic distillation method is the traditional separation and purification technology of these hydrocarbon mixtures, which not only requires high pressure and very low temperature but also consumes a lot of energy during the separation process. To date, the pressure swing adsorption process,[13] which is the most efficient and economical separation technology, has been widely developed. In this technology, porous adsorbents play a key role in the efficiency of separation because of their excellent adsorption capacity.

To be practical, porous adsorbents such as metal−organic frameworks (MOFs) and porous organic polymers (POPs) have shown excellent potential for CO_2 capture and the separation of light hydrocarbons (C_3H_8, C_2H_6 vs CH_4).[14−17] Compared with MOFs, various new kinds of POPs such as covalent organic frameworks,[18] conjugated microporous polymers,[19] polymers of intrinsic microporosity,[20] hyper-cross-linked polymers,[21] benzimidazole-linked polymers (BILPs),[22,23] porous aromatic frameworks (PAFs),[24] and covalent triazine frameworks (CTFs),[25,26] have shown higher mechanical, physical, and chemical stability. Meanwhile, the other advantages of POPs, including variable morphologies, large surface areas, and easy modification, make them easy to achieve high storage capacity and high selectivity. Researchers

Received: May 24, 2018
Accepted: July 18, 2018
Published: July 18, 2018

DOI: 10.1021/acsami.8b08625
ACS Appl. Mater. Interfaces 2018, 10, 26678−26686

can not only change the pore properties of POPs by selecting structurally different organic building blocks but also provide the affinity sites for particular gas by introducing different functional groups/sites, such as porphyrins,[17] benzimidazole,[22] carbazole,[27] Tröger's base,[28,29] and N-heterocyclic,[30] thereby increasing the preferential interaction of specific gases.

CTFs, as a representative class of POPs, were first synthesized through ionothermal polymerization by Thomas et al. in 2008.[25,26] Notably, not only do CTFs inherit the merits of POPs, but also the synthetic raw materials (cyanic monomers) of CTFs are easily obtained. In these polymerizations, $ZnCl_2$ is used as both catalyst and reaction solvent. Compared with the vast majority of POPs, the synthesis process of CTFs does not require expensive transition/noble metal catalysts, as well as anhydrous and inert conditions. These characteristics of CTFs make them be of great advantage in a wide range of applications such as sensing,[31] gas adsorption/separations,[32] photocatalysis,[33] electrode materials in supercapacitors,[34] or oxygen reduction reaction.[35] So far, researchers used a variety of strategies to build new types of CTFs for the purpose of increasing the adsorption capacity of CO_2. The introduction of nitrogen groups in aromatic cyano building blocks has proven to be a significant strategy to increase CO_2 capture, such as lutidine and pyrimidine building units,[36] pyridine,[37] and benzimidazole groups.[38] However, the fabrication of CTFs for the high-performance capture CO_2 and CO_2/CH_4, C_2H_6/CH_4, and C_3H_8/CH_4 selective separation remain few.

In this study, we successfully construct a series of highly porous covalent triazine frameworks (**CTF-BIBs**) by using 1,4-bis(5-cyano-1*H*-benzimidazole-2-yl)benzene (**BCBIB**) as building blocks. The longer molecular structure of **BCBIB** can increase the Brunauer–Emmett–Teller (BET) surface area of the obtained materials, and the N-rich building units provide CO_2 affinity sites. We investigated the effects of reaction temperature on physical porosity and gas adsorption properties of the obtained materials. Then, we carefully explored CO_2 sorption ability and selective separation for CO_2/N_2, CO_2/CH_4, C_2H_6/CH_4, and C_3H_8/CH_4. The highest uptake performances for CO_2 (97.6 $cm^3\ g^{-1}$) are observed for **CTF-BIB-1** at 273 K and 1 bar. Excitingly, the C_3H_8/CH_4 selectivity of **CTF-BIB-1** is up to 386.6 (298 K, 1 bar) by ideal adsorption solution theory (IAST), and it is the best separation performance in industrial fixed bed adsorbers by transient breakthrough simulations for equimolar $CO_2/C_3H_8/C_2H_6/CH_4$ mixture separation. This work demonstrates that the incorporation of bisbenzimidazole in the frameworks of CTFs will enhance the performance of gas adsorption for CO_2 and separation for small hydrocarbons.

EXPERIMENTAL SECTION

Synthesis of 1,4-Bis(5-cyano-1*H*-benzimidazole-2-yl)-benzene (BCBIB). In a 250 mL round-bottom flask, a solution of 3,4-diaminobenzonitrile (3.73 g, 28 mmol), 1,4-benzenedicarboxaldehyde (1.88 g, 14 mmol), and sodium hydrogen sulfite (4.20 g, 40 mmol) in *N*,*N*-dimethylacetamide (150 mL) was heated to 140 °C and stirred for 24 h. After cooling down to RT, deionized water (300 mL) was added into the reaction mixture, and then the solid formed was filtered off. Then, the product was washed with deionized water and dried under vacuum at 100 °C for 24 h, and recrystallization with dimethyl sulfoxide afforded **BCBIB** as a pale-yellow solid (yield, 3.52 g, 9.40 mmol, 69.8%). Elemental analysis (%): calcd C, 73.32; H, 3.36; N, 23.32. Found: C, 73.88; H, 3.71; N, 23.83. ^{1}H NMR (300 MHz, DMSO-d_6, δ, ppm): 13.61 (s, 2H), 8.39 (s, 4H), 8.17 (s, 2H), 7.76 (s, 2H), 7.61 (dd, J_1 = 8.3 Hz, J_2 = 1.4 Hz, 2H). HRMS (ESI): calcd for $C_{22}H_{13}N_6^+$ ($[M + H]^+$), 361.1196; found, 361.1196.

General Synthesis Procedure for CTF-BIBs. **BCBIB** (200 mg, 0.55 mmol) and anhydrous $ZnCl_2$ (605 mg, 4.44 mmol) were ground well and transferred into an ampoule under inert N_2 atmosphere. Then, the ampoule was sealed by pumping with a vacuum pump and placed into a furnace. The ampoule was calcined at 500 (**CTF-BIB-1**), 550 (**CTF-BIB-2**), or 600 °C (**CTF-BIB-3**) for 40 h with a heating ramp of 1 °C min^{-1}. When the ampoule dropped to room temperature, it was cautiously opened. The crude product was ground well and used numerous deionized to wash. Next, the excess $ZnCl_2$ was removed by stirring in 1 M HCl for 1 day. The resulting material was washed repeatedly many times using deionized water and ethanol and extracted by Soxhlet with tetrahydrofuran. In the end, the obtained black solid was dried under vacuum at 120 °C for 12 h. For comparison, **CTF-BIB-tf** was prepared in 1,2-dichloroethane solution by using the triflic acid catalyzed method.[32]

RESULTS AND DISCUSSION

Synthesis and Characterization of BCBIB. The bisbenzimidazole-functionalized aromatic dicyano building block **BCBIB** was synthesized with a good yield by the easy direct oxidative coupling reaction of 1,4-benzenedicarboxaldehyde and 3,4-diaminobenzonitrile (Figure S1). The chemical structure of **BCBIB** was approved by Fourier transform infrared (FT-IR) (Figure S2), ^{1}H NMR (Figure S3), and high-resolution mass spectrometry (HRMS) (Figure S4). In the FT-IR spectra, the strong adsorption located at about 3301 cm^{-1} can be assigned to the −NH of benzimidazole rings, and the strong adsorption peak located at near 1620 cm^{-1} (C═N) can be ascribed to the skeleton stretching of benzimidazole rings. At the same time, the characteristic absorption peaks near 2219 cm^{-1} can correspond to −CN groups. Simultaneously, in the ^{1}H NMR spectrum (Figure S3), the assignment of all protons is determined by the chemical shift and integral values. Also, in the HRMS spectrum, the molecular weight was precisely measured, and its chemical formula was analyzed. Finally, the thermogravimetric analysis (TGA) curve of **BCBIB** (Figure S5, Supporting Information) prior to the polymerization shows that the main weight loss starts near 450 °C, and then the benzimidazole rings begin to decompose. The good thermal stability of **BCBIB** ensures that the skeleton remains stable under continuous heating at high polymerization temperature, generally.

Synthesis and Characterization of CTF-BIBs. The synthesis of bisbenzimidazole-functionalized CTFs (denoted as **CTF-BIBs**) was carried out by using bisbenzimidazole containing monomer **BCBIB** through ionothermal polymerization, in which molten $ZnCl_2$ was used as the catalyst and reaction solvent (Scheme 1). To investigate the effect of the molar ratio of the $ZnCl_2$ to the monomer on the porosity properties of materials, three **CTF-BIBs** were synthesized at 500 °C by using 5, 8, and 10 equiv $ZnCl_2$. As shown in Figure S6 and Table S1, a 1:8 ratio of **BCBIB** and $ZnCl_2$ is an ideal condition for high surface areas and the highest porosity. Next, to systematically survey the influence of the synthetic temperature on porosity and gas adsorption, **CTF-BIB-1–3** were prepared in a sealed ampule for 40 h at 500, 550, and 600 °C, respectively. It should be paid more attention that when the sealed ampule was open, there were obviously positive pressures. This phenomenon was principally ascribed to the gas generated by the partial decomposition of the benzimidazole group at a high temperature.[38]

DOI: 10.1021/acsami.8b08625
ACS Appl. Mater. Interfaces 2018, 10, 26678–26686

Scheme 1. Synthesis Route and Idealized Structure of CTF-BIBs

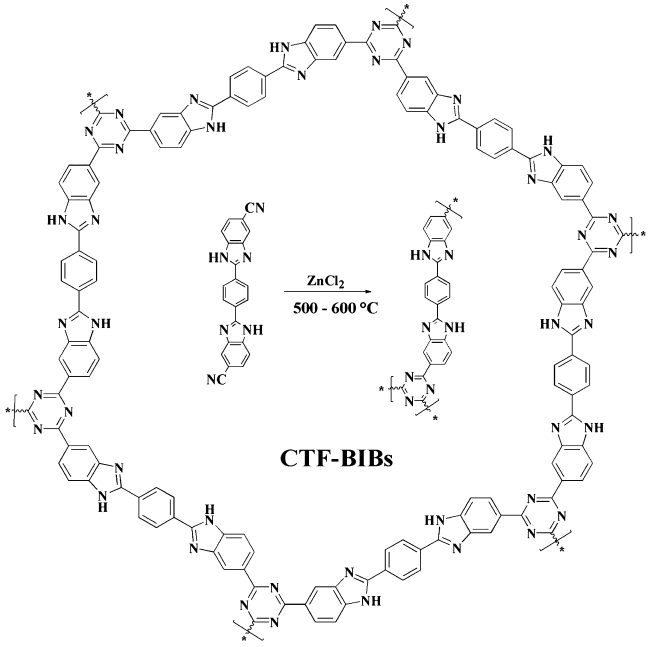

The successful polymerization reaction was confirmed by FT-IR analysis (Figure 1). The characteristic −CN peak of **BCBIB** at about 2219 cm^{-1} almost totally disappeared after ionothermal polymerization. Meanwhile, the characteristic peaks for triazine rings appeared at 1570 and 1371 cm^{-1} in all **CTF-BIBs**.[36,39] To obtain more detailed information about the chemical structures of the **CTF-BIBs**, solid-state ^{13}C NMR was carried out for all the materials (Figures S7−S9, Supporting Information). The characteristic peak near 126 ppm can be assigned to aromatic carbons. Meanwhile, the peaks around 152.8, 152.3, and 154.2 ppm in **CTF-BIB-1**, **CTF-BIB-2**, and **CTF-BIB-3** correspond to NC(Ph)N in benzimidazole units.[23,40] However, there is no way to distinguish the characteristic peak of carbon of triazine due to the partial graphitization of frameworks.[41,42] Next, the evolution of nitrogen functional groups during **CTF-BIBs** formation is confirmed by X-ray photoelectron spectroscopy (XPS). The binding energy of N 1s in **CTF-BIBs** was deconvoluted into four different peaks (Figure S10, Supporting Information): pyridinic N (398.13−398.30 eV), pyrrolic N (399.90−400.10 eV), graphitic N (401.08−401.24 eV), and oxidized N (402.47−402.60 eV).[43,44] The N 1s XPS spectra for **BCBIB** contain two configurations with the signal at 398.66 and 400.22 eV. The former corresponds to non-protonated pyridinic N, whereas binding energies at 400.22 eV are attributed to protonated pyrrolic nitrogen (−C−NH−C−) in the imidazole ring. After ionothermal polymerization, the obtainable **CTF-BIBs** contain two new nitrogen configurations, graphitic N and oxidized N. This may result from partial decomposition of the imidazole ring during the high reaction temperature, which is in great compliance with the FT-IR and solid-state ^{13}C NMR results as mentioned above. Therefore, when the temperature reaches 600 °C, the material is transformed into graphitized CTFs.

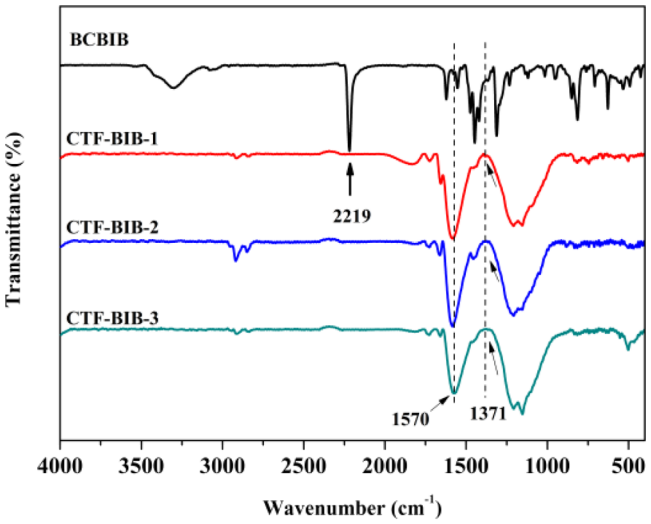

Figure 1. FT-IR spectra of the monomer **BCBIB** and **CTF-BIB-1−3**.

The crystalline nature of **CTF-BIBs** was confirmed by powder X-ray diffraction (PXRD) analysis (Figure S11, Supporting Information). The diffractograms show a broad diffraction peak around 24.7°, which suggests a generally amorphous structure. The morphologies of the samples were observed by scanning electron microscopy (SEM). As shown in Figures S12−S14 (Supporting Information), **CTF-BIBs** are composed of different sizes and aggregated particles with irregular shapes and rough surfaces. The transmission electron microscopy (TEM) images of **CTF-BIBs** shown in Figures S15−S17 (Supporting Information) demonstrate their disordered porous layered structure, which is identical to the abovementioned PXRD results. The thermal stabilities of the triazine frameworks play an important role in its applications, which was characterized by TGA under N_2 atmosphere (Figures S18−S20, Supporting Information). All **CTF-BIBs**

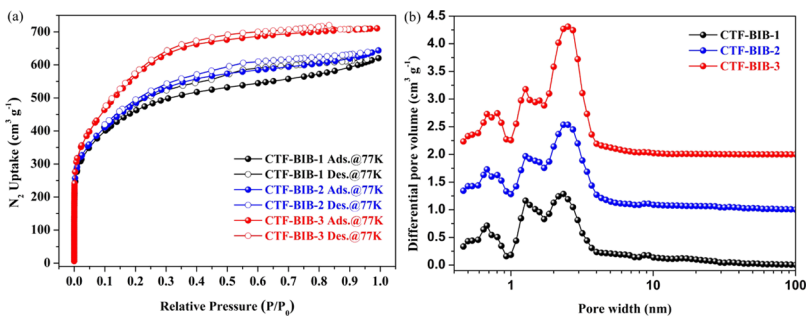

Figure 2. (a) N_2 sorption isotherms for **CTF-BIB-1** (black), **CTF-BIB-2** (blue), and **CTF-BIB-3** (red) at 77 K; (b) PSD curve of **CTF-BIB-1** (black), **CTF-BIB-2** (blue), and **CTF-BIB-3** (red) from N_2 adsorption at 77 K using the NLDFT method.

DOI: 10.1021/acsami.8b08625
ACS Appl. Mater. Interfaces 2018, 10, 26678−26686

Table 1. Pore Characteristics of CTF-BIBs

CTF-BIBs	reaction conditions	S_{BET} [a] (m^2 g^{-1})	V_{mic} [b] (cm^3 g^{-1})	V_{tot} [c] (cm^3 g^{-1})	V_{micro}/V_{tot}
CTF-BIB-1	500 °C/40 h	1636	0.63	0.96	0.66
CTF-BIB-2	550 °C/40 h	1714	0.68	0.99	0.69
CTF-BIB-3	600 °C/40 h	2088	0.86	1.10	0.78

[a]BET surface area. [b]Micropore volume calculated from N_2 adsorption isotherms using the *t*-plot method. [c]Total pore volume at P/P_o = 0.99.

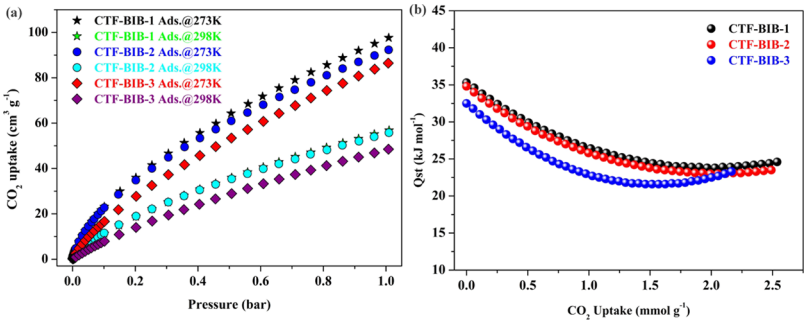

Figure 3. (a) Gas sorption isotherms of CO_2 for **CTF-BIBs** measured at 273 and 298 K under 1 bar and (b) calculated isosteric heats of CO_2 adsorption for **CTF-BIBs**.

Table 2. Sorption Results for Each CTF-BIB Including Sorption Capacities and Sorption Selectivities[a]

	gas uptake (cm^3 g^{-1}, 1 bar)					selectivity (IAST)			
CTF-BIBs	CO_2	C_3H_8	C_2H_6	CH_4	N_2	CO_2/CH_4	CO_2/N_2	C_3H_8/CH_4	C_2H_6/CH_4
CTF-BIB-1	97.6/56.8	209.2/158.1	132.1/91.1	30.3/16.2	10.3/5.1	6.9 (6.8)	29.3	386.6	20.4
CTF-BIB-2	92.3/55.6	206.7/157.7	133.4/91.2	31.9/17.5	10.0/5.3	6.9 (7.3)	33.1	311.2	19.6
CTF-BIB-3	86.4/48.5	232.1/167.5	136.5/90.2	27.3/16.2	9.8/3.9	4.6 (4.7)	21.2	170.5	13.6

[a]CO_2, C_3H_8, C_2H_6, and CH_4 sorption was measured at 273/298 K at 1 bar; CO_2/CH_4 (0.5/0.5 and 0.05/0.95), CO_2/N_2 (0.15/0.85), C_3H_8/CH_4 (0.5/0.5), and C_2H_6/CH_4 (0.5/0.5) selectivities calculated by the IAST method at 298 K and 1 bar, respectively.

reveal high thermal stability, and the onset decomposition temperature is around 450 °C. The slight weight mass loss before 100 °C is attributed to the adsorption of gas and water vapor within the framework structure, which is in accordance with most of the reported POPs.[38] Inductively coupled plasma (ICP) spectral analyses show 0.19, 0.12, and 0.20 wt % zinc contents for **CTF-BIB-1**, **CTF-BIB-2**, and **CTF-BIB-3**, respectively, which is a low and reasonable quantity of Zn ions.[45,46]

Porosity Measurements. The porosity properties such as the BET surface areas, pore volume, and pore size distribution (PSD) of **CTF-BIBs** synthesized at different temperatures were characterized by nitrogen adsorption measurements at 77 K. The corresponding N_2 adsorption and desorption isotherms and PSDs of **CTF-BIBs** are shown in Figure 2. For **CTF-BIBs**, the isotherms show rapid nitrogen increases in the low relative pressure region (P/P_o < 0.01), representing a typically microporous structure. Meanwhile, the low-pressure hysteresis loops are found for all triazine frameworks, indicating the existence of the mesopores in these **CTF-BIBs**. According to the IUPAC classification, the synthesized **CTF-BIBs** displayed type I N_2 sorption isotherms with a type IV character.[47] The BET surface areas of **CTF-BIB-1**−**3** are 1636, 1714, and 2088 m^2 g^{-1}, respectively. The total pore volumes (V_{tot}) of **CTF-BIB-1** to **CTF-BIB-3** determined by using the single point measurement of the N_2 adsorbed at P/P_o = 0.99 are 0.96, 0.99, and 1.10 cm^3 g^{-1}, respectively. It is noteworthy that the BET surface area and total pore volume of the obtained materials increased gradually as the reaction temperature increased. These can be ascribed to the fact that high temperature causes more defects derived from the decomposition of the benzimidazole rings or triazine rings in the framework.[38,48] The BET surface areas of synthesized **CTF-BIBs** are higher than those reported for CTF-BIs (642−1549 m^2 g^{-1}),[38] which may be attributed to the increased length of organic monomers and the optimized synthesis conditions. The PSDs of **CTF-BIBs** were calculated using the nonlocal density functional theory (NLDFT) method (Figure 2b). These detailed pore characteristics are summarized in Table 1. For **CTF-BIBs**, the micropores are mainly concentrated in two peaks at 0.68 and 1.27 nm, whereas the small mesopores with a dominant pore size are found at 2.5 nm, which reveal that **CTF-BIBs** have both microporous and mesoporous features. **CTF-BIB-tf** was prepared in 1,2-dichloroethane solution by using the triflic acid catalyzed method. The porous properties of **CTF-BIB-tf** were characterized by nitrogen adsorption measurements at 77 K (Figure S21). Unfortunately, **CTF-BIB-tf** does not show any N_2 uptakes.

Gas Adsorption Behaviors for CO_2 and Light Hydrocarbons. The synthesized **CTF-BIBs** possess high surface area, excellent physical−chemical stability, π-conjugated triazine rings, as well as the CO_2-philic benzimidazoles. Considering these features, the CO_2 adsorption properties of these **CTF-BIBs** have been investigated. The CO_2 adsorption−desorption isotherms at 273 and 298 K are displayed in Figure 3a. The CO_2 uptake values are 97.6 cm^3 g^{-1} (4.35 mmol g^{-1}) for **CTF-BIB-1**, 92.3 cm^3 g^{-1} (4.12 mmol g^{-1}) for **CTF-BIB-2**, and 86.4 cm^3 g^{-1} (3.86 mmol g^{-1}) for **CTF-BIB-3** under 1 bar at 273 K, whereas 56.8 cm^3 g^{-1} (2.54 mmol g^{-1}), 55.6 cm^3 g^{-1} (2.48 mmol g^{-1}), and 48.5 cm^3 g^{-1} (2.17 mmol

DOI: 10.1021/acsami.8b08625
ACS Appl. Mater. Interfaces 2018, 10, 26678−26686

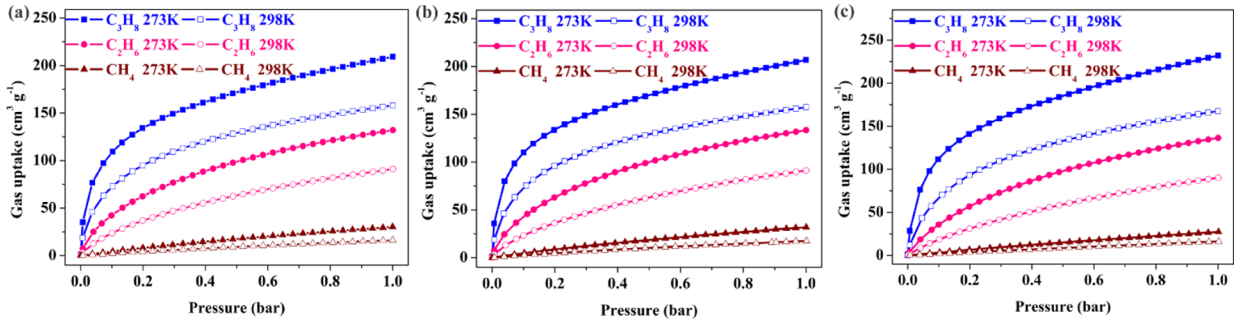

Figure 4. Gas sorption isotherms of C_3H_8, C_2H_6, and CH_4 for **CTF-BIB-1** (a), **CTF-BIB-2** (b), and **CTF-BIB-3** (c) measured at 273 and 298 K under 1 bar.

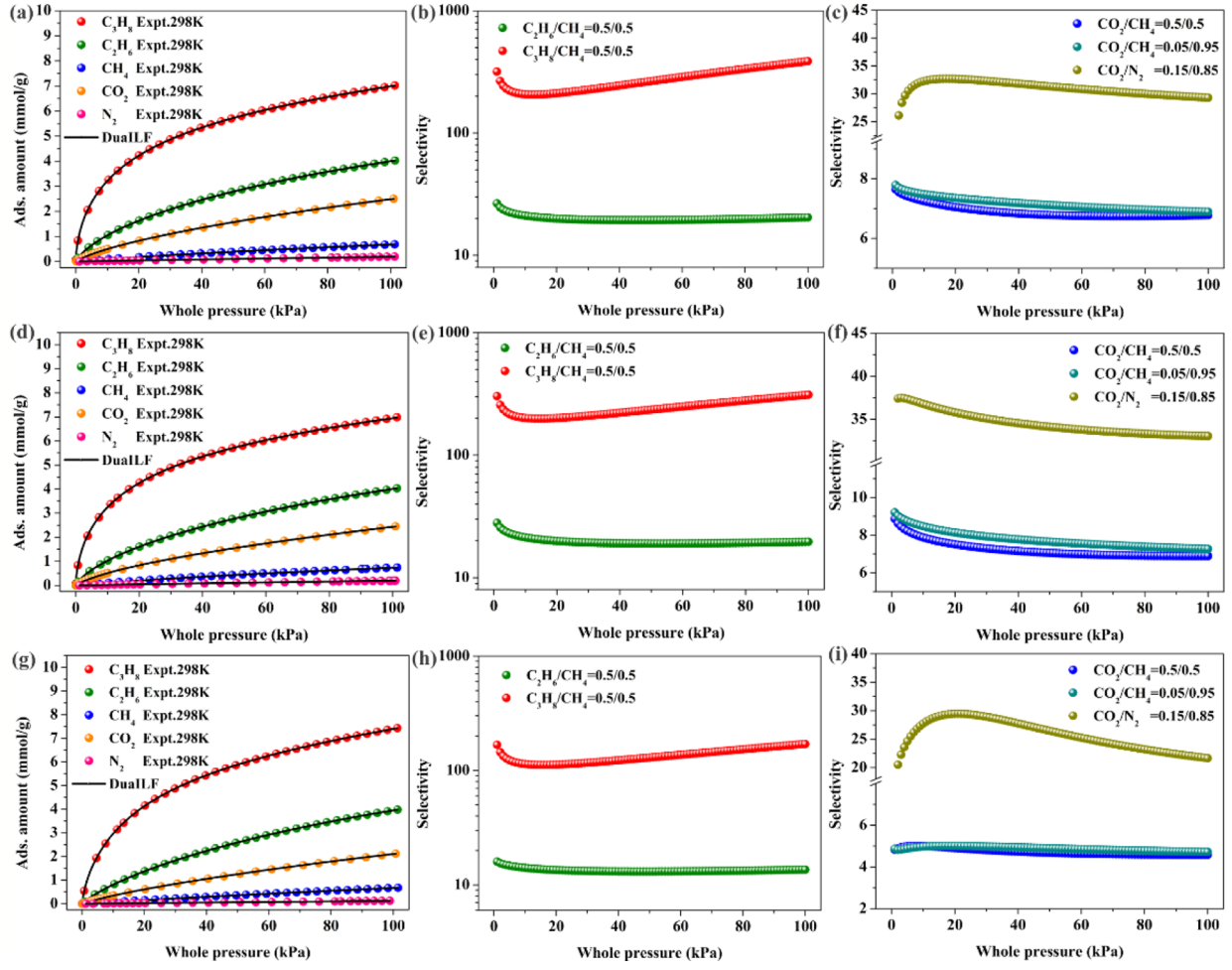

Figure 5. N_2, CO_2, CH_4, C_2H_6, and C_3H_8 sorption isotherms at 298 K and 1 bar by using the DSLF equation fitting [(a) **CTF-BIB-1**, (d) **CTF-BIB-2**, (g) **CTF-BIB-3**]; the adsorption selectivities are calculated by IAST at 298 K and 1 bar [(b,c) **CTF-BIB-1**, (e,f) **CTF-BIB-2**, (h,i) **CTF-BIB-3**].

g^{-1}) for **CTF-BIB-1−3** at 298 K (Table 2). The CO_2 uptake of **CTF-BIB-1** (2.54 mmol g^{-1}) is higher than those of many reported CTFs measured at 298 K and 1 bar, such as CTF-1 (1.41 mmol g^{-1}),[49] fl-CTFs (0.71−2.29 mmol g^{-1}),[50] CTF-TBs (1.50−2.46 mmol g^{-1} at 303 K),[51] PHCTFs (1.23−1.57 mmol g^{-1}),[45] and CTF-20-400 (2.09 mmol g^{-1}),[52] even compared with other kinds of benchmark materials, the zeolite 13X (3.5 mmol g^{-1}),[4] polyethylenimine-modified conventional silica (2.4 mmol g^{-1}),[6] and the commercially available BPL carbon (2.08 mmol g^{-1}).[53] Interestingly, the CO_2 uptake values of **CTF-BIBs** are also comparable to reported CTF-BIs with benzimidazole rings (1.67−2.73 mmol g^{-1}, at 303 K and 1.1 bar).[38] It is worth noticing that the BET surface area of **CTF-BIB-3** is higher than that of **CTF-BIB-1**, but the CO_2 uptake values of **CTF-BIB-3** are lower.

This phenomenon demonstrates the CO_2 uptake values is not only corresponding to the BET surface areas. The reason can be ascribed to the fact that high reaction temperature leads to partial decomposition or fragmentation of benzimidazole and triazine rings in **CTF-BIBs**, lowering the affinity between framework and CO_2 molecules. Elemental analysis measurements and N/C molar ratios also confirmed this fact (Table

DOI: 10.1021/acsami.8b08625
ACS Appl. Mater. Interfaces 2018, 10, 26678−26686

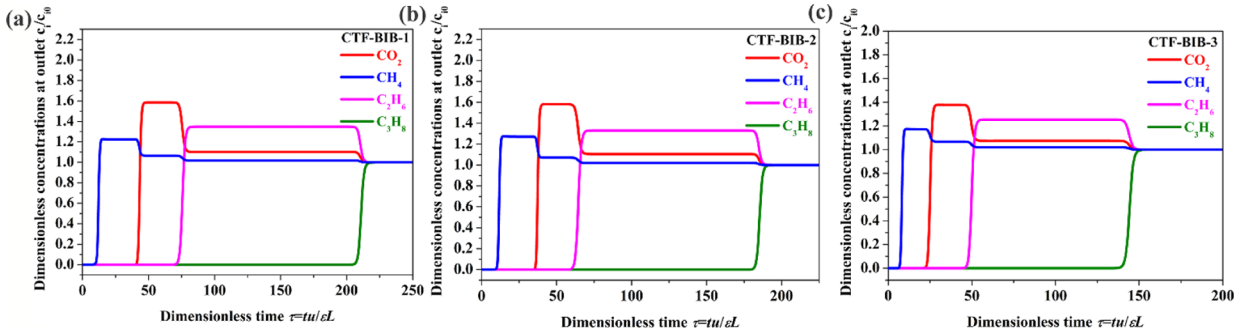

Figure 6. Transient breakthrough simulation data for the equimolar 4-component $CO_2/CH_4/C_2H_6/C_3H_8$ mixture at 100 kPa and 298 K of **CTF-BIB-1** (a), **CTF-BIB-2** (b), and **CTF-BIB-3** (c).

S2). The nitrogen contents of **CTF-BIBs** significantly decrease with increasing reaction temperature, where **CTF-BIB-3** is far less than the theoretical values. Meanwhile, the N/C molar ratios of **CTF-BIB-1**, **CTF-BIB-2**, and **CTF-BIB-3** are 15.7, 12.1, and 11.5%, respectively, which are lower than theoretical values (27.3%). The isosteric heat (Q_{st}) values of CO_2 adsorption can reflect the interaction strength between the frameworks and CO_2, which are calculated by using the virial equation to fit the CO_2 adsorption isotherms at 273 and 298 K (Figures 3b and S22). The Q_{st} values of **CTF-BIB-1**, **CTF-BIB-2**, and **CTF-BIB-3** at zero coverage are 35.2, 34.7, and 32.5 kJ mol^{-1}, respectively, suggesting relatively strong CO_2-network interactions. The adsorption enthalpies of **CTF-BIB-1** and **CTF-BIB-2** are quite similar, which can be attributed to their almost similar pore volume and BET surface area. The Q_{st} values of **CTF-BIBs** are higher than those of most porous solid-state adsorbents, such as CTF-1 (27.5 kJ mol^{-1}),[49] BILPs (26.7−28.8 kJ mol^{-1}),[22,23,40] PAF-1 (15.6 kJ mol^{-1}),[54] activated carbons (e.g., BPL 25.7 kJ mol^{-1}, A10 21.6 kJ mol^{-1}, Maxsorb 16.2 kJ mol^{-1}),[55] and APOPs (26.6−33.3 kJ mol^{-1}).[56] The high Q_{st} value of **CTF-BIBs** can be attributed to the micropore structure effect, as well as rich CO_2 affinity positions.

To further evaluate storage capacity of small hydrocarbons (C1−C3), the single component adsorption isotherms of CH_4, C_2H_6, and C_3H_8 are measured at 273 and 298 K under 1 bar, respectively (Figure 4a−c). As expected, **CTF-BIB-1**, **CTF-BIB-2**, and **CTF-BIB-3** display similar adsorption isotherms. The rapidly improved amounts of small hydrocarbons (C1−C3) were adsorbed at low relative pressures; it was followed by the progressive increase of their adsorption with the applied pressure, eventually leveling off. The adsorption capacities of all **CTF-BIBs** are summarized in Table 2. All the porous **CTF-BIBs** possess higher C_3H_8 and C_2H_6 uptakes than that of CH_4 because of the presence of small mesopores in the frameworks. Among all **CTF-BIBs**, **CTF-BIB-3** has the highest C_3H_8 (232.1/167.5 $cm^3\ g^{-1}$) and C_2H_6 (136.5/90.2 $cm^3\ g^{-1}$) adsorption capacity at 273/298 K, outperforming that of some previously reported porous materials such as JLU-Liu-18 (138/116 $cm^3\ g^{-1}$ for C_3H_8 and 128/92 $cm^3\ g^{-1}$ for C_2H_6 at 273/298 K),[10] ZnP-CTF-400 (112 $cm^3\ g^{-1}$ for C_3H_8 and 70 $cm^3\ g^{-1}$ for C_2H_6 at 298 K),[57] and MFM-202a (151.4 $cm^3\ g^{-1}$ for C_3H_8 and 94.3 $cm^3\ g^{-1}$ for C_2H_6 at 293 K).[58] The same method is used to calculate the isosteric heat (Q_{st}) values of small (C1−C3) hydrocarbon adsorption by using the virial equation to fit the adsorption isotherms at 273 and 298 K (Figures S23−S25). The Q_{st} values of C_3H_8, C_2H_6, and CH_4 for **CTF-BIB-1** at zero coverage are 37.6, 30.7, and 20.5 kJ mol^{-1}; for **CTF-BIB-2**, they are 37.2, 34.2, and 20.4 kJ mol^{-1}; and for **CTF-BIB-3**, they are 39.0, 27.8, and 17.4 kJ mol^{-1}, respectively. The quantitative relation of Q_{st} values for small hydrocarbon is C_3H_8 > CH_4 and C_2H_6 > CH_4, revealing that **CTF-BIBs** possess extremely promising prospect for highly selective adsorption separation of C_3H_8 and C_2H_6 over CH_4.

Gas Separation Behaviors. Considering the high CO_2 adsorption properties and great binding affinity of **CTF-BIB** materials, the adsorption selectivities of CO_2/CH_4 (0.5/0.5 and 0.05/0.95) and CO_2/N_2 (0.15/0.85) were further evaluated by IAST. The models are built very well (R^2 > 0.999) to fit the experimental single-component isotherms at 298 K and 1 bar through the dual-site Langmuir−Freundlich (DSLF) equation (Figure 5). Then, we used the fitting parameters to predict polycomponent adsorption by IAST (listed in Table S3). All calculation results are shown in Table 2. The selectivities of CO_2 over CH_4 (0.5/0.5 and 0.05/0.95) for **CTF-BIB-1** according to the experimental data are 6.9 and 6.8; for **CTF-BIB-2**, they are 6.9 and 7.3; and for **CTF-BIB-3**, they are 4.6 and 4.7, respectively, which are comparable or only slightly lower than those of CTF-DCBT (10.3 at equimolar and 298 K),[46] JLU-SOF1-R (3.9 at equimolar and 298 K),[59] BILP-11 to 13 (6.6−7.6 at a ratio of 0.05/0.95 and 298 K),[60] PIN-1 to 2 (5 at equimolar and 298 K),[61] and CTF-DCN-500 (5 at equimolar and 298 K).[62] The CO_2/N_2 adsorption selectivity for **CTF-BIB-1**, **CTF-BIB-2**, and **CTF-BIB-3** are 29.3, 33.1, and 21.2, respectively, which are comparable to recent work, such as fl-CTF350 (23),[50] PIN-1 (31),[61] CTF-DCN-500 (37),[62] and ALP-1 to 4 (26−35).[63] These results illustrate that bisbenzimidazole-functionalized **CTF-BIBs** are promising candidates for CO_2 capture and separation.

The present separation of hydrocarbons is one of the important industrial applications. To achieve this aim, the selectivity of equimolar mixtures C_2H_6/CH_4, and C_3H_8/CH_4 for **CTF-BIBs** was calculated by IAST (Figure 5). The obtained values of selectivities of C_2H_6 over CH_4 for **CTF-BIB-1**, **CTF-BIB-2**, and **CTF-BIB-3** are 20.4, 19.6, and 13.6, respectively. On the basis of the high selectivities of **CTF-BIBs**, the separation of C_2H_6 from natural gas becomes highly probable. The obtained values of the selectivities of C_3H_8 over CH_4 for **CTF-BIB-1**, **CTF-BIB-2**, and **CTF-BIB-3** are 386.6, 311.2, and 170.5, respectively. The C_3H_8/CH_4 selectivity of **CTF-BIB-1** is much higher than **CTF-BIB-3**. This can be ascribed to the higher N content and the more complete framework structure of **CTF-BIB-1**, which enhance the host−guest interaction. The very high C_3H_8/CH_4 selectivity of **CTF-BIB-1** is significantly higher than PAF-40-Mn (246),[17] NAC-800 (203.6),[64] UTSA-35a (80),[65] Zr-BDC (168.7),[66] and Zr-

DOI: 10.1021/acsami.8b08625
ACS Appl. Mater. Interfaces 2018, 10, 26678−26686

1,4-NDC (247.1).[66] The reason for the high C_3H_8/CH_4 selectivity is that ultrahigh C_3H_8 adsorption and excellent affinity, compared to those of CH_4. These results reveal that the obtained **CTF-BIBs** have good potential applications for CO_2 capture and sorption separation of small hydrocarbons.

Breakthrough Simulation Properties. The separation performance of industrial fixed bed adsorbents is determined not merely by the adsorption selectivities of porous materials but also by their uptake capacity. For an appropriate evaluation of the combined effects of adsorption selectivity and uptake capacity of **CTF-BIBs**, transient breakthrough simulations were carried out for equimolar $CO_2/C_3H_8/C_2H_6/CH_4$ mixtures operating at a total pressure of 100 kPa and 298 K (Figure 6), using the methodology described in earlier publications.[67−70] It could be observed that the breakthrough times sequence is C_3H_8 > C_2H_6 > CO_2 > CH_4, which is decided by the hierarchy of adsorption strengths. The breakthrough times for **CTF-BIB-1** are higher than others, and **CTF-BIB-1** has the best separation performance. These results are consistent with selectivities by IAST calculations. It is also worth noting that there is a time interval in the breakthroughs, and it appears that **CTF-BIBs** are suitable for purifying natural gas by separating each of the four component gas mixtures in a nearly pure form.

CONCLUSIONS

In conclusion, we have successfully synthesized a series of highly porous covalent triazine frameworks (**CTF-BIBs**) by using 1,4-bis(5-cyano-1*H*-benzimidazole-2-yl)benzene (**BCBIB**) as building blocks. We also investigated the effects of reaction temperature on physical porosity and gas adsorption properties of the obtained materials. The BET surface areas of **CTF-BIBs** are high up to 2088 $m^2\ g^{-1}$. Meanwhile, these **CTF-BIBs** exhibit extraordinary CO_2 and small hydrocarbon (C1−C3) sorption ability, and excellent selective separation for CO_2/N_2, CO_2/CH_4, C_2H_6/CH_4, and C_3H_8/CH_4. In particular, the CO_2 uptake capacity of **CTF-BIB-1** is up to 97.6 $cm^3\ g^{-1}$ (4.35 mmol g^{-1}) at 273 K and 56.8 $cm^3\ g^{-1}$ (2.54 mmol g^{-1}) at 298 K under 1 bar, and the high C_3H_8/CH_4 selectivity is 386.6 at 298 K and 1 bar. Meanwhile, **CTF-BIB-1** displays excellent separation performance in industrial fixed bed adsorbers by transient breakthrough simulations for equimolar $CO_2/C_3H_8/C_2H_6/CH_4$ mixture separation. Because of their high gas uptake capacity and adsorption selectivity, **CTF-BIBs** show promising application prospect in CO_2 capture and adsorptive separation of small hydrocarbon applications.

ASSOCIATED CONTENT

Supporting Information

The Supporting Information is available free of charge on the ACS Publications website at DOI: 10.1021/acsami.8b08625.

Experimental details, PXRD, SEM, TEM, TGA, ICP, NMR, XPS, gas adsorption isotherms, and breakthrough simulations (PDF)

AUTHOR INFORMATION

Corresponding Authors

*E-mail: xiaoweisong@jlu.edu.cn (X.S.).
*E-mail: liangzq@jlu.edu.cn (Z.L.).

ORCID

Rajamani Krishna: 0000-0002-4784-8530
Yue Yu: 0000-0002-8189-2291
Yunling Liu: 0000-0001-5040-6816
Zhiqiang Liang: 0000-0003-4473-8544

Notes

The authors declare no competing financial interest.

ACKNOWLEDGMENTS

We thank the National Natural Science Foundation of China (grant nos. 21471064 and 21621001), the National Key Research and Development Program of China (grant no. 2016YFB0701100), and the 111 project of the Ministry of Education of China (grant no. B17020) for supporting this work.

REFERENCES

(1) Haszeldine, R. S. Carbon Capture and Storage: How Green Can Black Be? *Science* **2009**, *325*, 1647−1652.
(2) Goeppert, A.; Czaun, M.; Surya Prakash, G. K.; Olah, G. A. Air as the renewable carbon source of the future: an overview of CO2 capture from the atmosphere. *Energy Environ. Sci.* **2012**, *5*, 7833−7853.
(3) Rochelle, G. T. Amine Scrubbing for CO2 Capture. *Science* **2009**, *325*, 1652−1654.
(4) Choi, S.; Drese, J. H.; Jones, C. W. Adsorbent Materials for Carbon Dioxide Capture from Large Anthropogenic Point Sources. *ChemSusChem* **2009**, *2*, 796−854.
(5) Wang, Q.; Luo, J.; Zhong, Z.; Borgna, A. CO2 capture by solid adsorbents and their applications: current status and new trends. *Energy Environ. Sci.* **2011**, *4*, 42−55.
(6) Wang, J.; Huang, L.; Yang, R.; Zhang, Z.; Wu, J.; Gao, Y.; Wang, Q.; O'Hare, D.; Zhong, Z. Recent advances in solid sorbents for CO2 capture and new development trends. *Energy Environ. Sci.* **2014**, *7*, 3478−3518.
(7) He, Y.; Zhou, W.; Qian, G.; Chen, B. Methane Storage in Metal-Organic Frameworks. *Chem. Soc. Rev.* **2014**, *43*, 5657−5678.
(8) Makal, T. A.; Li, J.-R.; Lu, W.; Zhou, H.-C. Methane Storage in Advanced Porous Materials. *Chem. Soc. Rev.* **2012**, *41*, 7761−7779.
(9) Sikdar, N.; Bonakala, S.; Haldar, R.; Balasubramanian, S.; Maji, T. K. Dynamic Entangled Porous Framework for Hydrocarbon (C2-C3) Storage, CO2 Capture, and Separation. *Chem.—Eur. J.* **2016**, *22*, 6059−6070.
(10) Yao, S.; Wang, D.; Cao, Y.; Li, G.; Huo, Q.; Liu, Y. Two Stable 3D Porous Metal-Organic Frameworks with High Performance for Gas Adsorption and Separation. *J. Mater. Chem. A* **2015**, *3*, 16627−16632.
(11) Nugent, P.; Belmabkhout, Y.; Burd, S. D.; Cairns, A. J.; Luebke, R.; Forrest, K.; Pham, T.; Ma, S.; Space, B.; Wojtas, L.; Eddaoudi, M.; Zaworotko, M. J. Porous materials with optimal adsorption thermodynamics and kinetics for CO2 separation. *Nature* **2013**, *495*, 80−84.
(12) Oschatz, M.; Antonietti, M. A search for selectivity to enable CO2 capture with porous adsorbents. *Energy Environ. Sci.* **2018**, *11*, 57−70.
(13) Jarvelin, H.; Fair, J. R. Adsorptive Separation of Propylene-Propane Mixtures. *Ind. Eng. Chem. Res.* **1993**, *32*, 2201−2207.
(14) Wilmer, C. E.; Farha, O. K.; Bae, Y.-S.; Hupp, J. T.; Snurr, R. Q. Structure-Property Relationships of Porous Materials for Carbon Dioxide Separation and Capture. *Energy Environ. Sci.* **2012**, *5*, 9849−9856.
(15) Liu, J.; Thallapally, P. K.; McGrail, B. P.; Brown, D. R.; Liu, J. Progress in adsorption-based CO2capture by metal-organic frameworks. *Chem. Soc. Rev.* **2012**, *41*, 2308−2322.
(16) He, Y.; Krishna, R.; Chen, B. Metal-Organic Frameworks with Potential for Energy-Efficient Adsorptive Separation of Light Hydrocarbons. *Energy Environ. Sci.* **2012**, *5*, 9107−9120.

(17) Meng, S.; Ma, H.; Jiang, L.; Ren, H.; Zhu, G. A Facile Approach to Prepare Porphyrinic Porous Aromatic Frameworks for Small Hydrocarbon Separation. *J. Mater. Chem. A* **2014**, *2*, 14536−14541.
(18) Cote, A. P.; Benin, A. I.; Ockwig, N. W.; O'Keeffe, M.; Matzger, A. J.; Yaghi, O. M. Porous, Crystalline, Covalent Organic Frameworks. *Science* **2005**, *310*, 1166−1170.
(19) Jiang, J.-X.; Su, F.; Trewin, A.; Wood, C. D.; Campbell, N. L.; Niu, H.; Dickinson, C.; Ganin, A. Y.; Rosseinsky, M. J.; Khimyak, Y. Z.; Cooper, A. I. Conjugated Microporous Poly(aryleneethynylene) Networks. *Angew. Chem., Int. Ed.* **2007**, *46*, 8574−8578.
(20) Yi, S.; Ma, X.; Pinnau, I.; Koros, W. J. A High-Performance Hydroxyl-Functionalized Polymer of Intrinsic Microporosity for An Environmentally Attractive Membrane-Based Approach to Decontamination of Sour Natural Gas. *J. Mater. Chem. A* **2015**, *3*, 22794−22806.
(21) Germain, J.; Hradil, J.; Fréchet, J. M. J.; Svec, F. High Surface Area Nanoporous Polymers for Reversible Hydrogen Storage. *Chem. Mater.* **2006**, *18*, 4430−4435.
(22) Rabbani, M. G.; El-Kaderi, H. M. Template-Free Synthesis of a Highly Porous Benzimidazole-Linked Polymer for CO2Capture and H2Storage. *Chem. Mater.* **2011**, *23*, 1650−1653.
(23) Rabbani, M. G.; El-Kaderi, H. M. Synthesis and Characterization of Porous Benzimidazole-Linked Polymers and Their Performance in Small Gas Storage and Selective Uptake. *Chem. Mater.* **2012**, *24*, 1511−1517.
(24) Ben, T.; Ren, H.; Ma, S.; Cao, D.; Lan, J.; Jing, X.; Wang, W.; Xu, J.; Deng, F.; Simmons, J. M.; Qiu, S.; Zhu, G. Targeted Synthesis of a Porous Aromatic Framework with High Stability and Exceptionally High Surface Area. *Angew. Chem., Int. Ed.* **2009**, *48*, 9457−9460.
(25) Kuhn, P.; Antonietti, M.; Thomas, A. Porous, Covalent Triazine-based Frameworks Prepared by Ionothermal Synthesis. *Angew. Chem., Int. Ed.* **2008**, *47*, 3450−3453.
(26) Kuhn, P.; Forget, A.; Su, D.; Thomas, A.; Antonietti, M. From Microporous Regular Frameworks to Mesoporous Materials with Ultrahigh surface Area: Dynamic Reorganization of Porous Polymer Networks. *J. Am. Chem. Soc.* **2008**, *130*, 13333−13337.
(27) Chen, Q.; Luo, M.; Hammershøj, P.; Zhou, D.; Han, Y.; Laursen, B. W.; Yan, C.-G.; Han, B.-H. Microporous Polycarbazole with High Specific Surface Area for Gas Storage and Separation. *J. Am. Chem. Soc.* **2012**, *134*, 6084−6087.
(28) Cui, Y.; Liu, Y.; Liu, J.; Du, J.; Yu, Y.; Wang, S.; Liang, Z.; Yu, J. Multifunctional porous Tröger's base polymers with tetraphenylethene units: CO2 adsorption, luminescence and sensing properties. *Polym. Chem.* **2017**, *8*, 4842−4848.
(29) Byun, J.; Je, S.-H.; Patel, H. A.; Coskun, A.; Yavuz, C. T. Nanoporous covalent organic polymers incorporating Tröger's base functionalities for enhanced CO2capture. *J. Mater. Chem. A* **2014**, *2*, 12507−12512.
(30) Dong, J.; Wang, Y.; Liu, G.; Cheng, Y.; Zhao, D. Isoreticular Covalent Organic Frameworks for Hydrocarbon Uptake and Separation: the Important Role of Monomer Planarity. *CrystEngComm* **2017**, *19*, 4899−4904.
(31) Bhunia, A.; Esquivel, D.; Dey, S.; Fernández-Terán, R.; Goto, Y.; Inagaki, S.; Van Der Voort, P.; Janiak, C. A photoluminescent covalent triazine framework: CO2 adsorption, light-driven hydrogen evolution and sensing of nitroaromatics. *J. Mater. Chem. A* **2016**, *4*, 13450−13457.
(32) Ren, S.; Bojdys, M. J.; Dawson, R.; Laybourn, A.; Khimyak, Y. Z.; Adams, D. J.; Cooper, A. I. Porous, Fluorescent, Covalent Triazine-Based Frameworks Via Room-Temperature and Microwave-Assisted Synthesis. *Adv. Mater.* **2012**, *24*, 2357−2361.
(33) Zhang, G.; Lan, Z.-A.; Wang, X. Conjugated Polymers: Catalysts for Photocatalytic Hydrogen Evolution. *Angew. Chem., Int. Ed.* **2016**, *55*, 15712−15727.
(34) Hao, L.; Ning, J.; Luo, B.; Wang, B.; Zhang, Y.; Tang, Z.; Yang, J.; Thomas, A.; Zhi, L. Structural Evolution of 2D Microporous Covalent Triazine-Based Framework toward the Study of High-Performance Supercapacitors. *J. Am. Chem. Soc.* **2015**, *137*, 219−225.
(35) Kamiya, K.; Kamai, R.; Hashimoto, K.; Nakanishi, S. Platinum-Modified Covalent Triazine Frameworks Hybridized with Carbon Nanoparticles as Methanol-Tolerant Oxygen Reduction Electrocatalysts. *Nat. Commun.* **2014**, *5*, 5040.
(36) Hug, S.; Stegbauer, L.; Oh, H.; Hirscher, M.; Lotsch, B. V. Nitrogen-Rich Covalent Triazine Frameworks as High-Performance Platforms for Selective Carbon Capture and Storage. *Chem. Mater.* **2015**, *27*, 8001−8010.
(37) Tuci, G.; Pilaski, M.; Ba, H.; Rossin, A.; Luconi, L.; Caporali, S.; Pham-Huu, C.; Palkovits, R.; Giambastiani, G. Unraveling Surface Basicity and Bulk Morphology Relationship on Covalent Triazine Frameworks with Unique Catalytic and Gas Adsorption Properties. *Adv. Funct. Mater.* **2017**, *27*, 1605672.
(38) Tao, L.; Niu, F.; Wang, C.; Liu, J.; Wang, T.; Wang, Q. Benzimidazole functionalized covalent triazine frameworks for CO2 capture. *J. Mater. Chem. A* **2016**, *4*, 11812−11820.
(39) Wu, S.; Liu, Y.; Yu, G.; Guan, J.; Pan, C.; Du, Y.; Xiong, X.; Wang, Z. Facile Preparation of Dibenzoheterocycle-Functional Nanoporous Polymeric Networks with High Gas Uptake Capacities. *Macromolecules* **2014**, *47*, 2875−2882.
(40) Rabbani, M. G.; Reich, T. E.; Kassab, R. M.; Jackson, K. T.; El-Kaderi, H. M. High CO2uptake and selectivity by triptycene-derived benzimidazole-linked polymers. *Chem. Commun.* **2012**, *48*, 1141−1143.
(41) Gu, C.; Liu, D.; Huang, W.; Liu, J.; Yang, R. Synthesis of covalent triazine-based frameworks with high CO2 adsorption and selectivity. *Polym. Chem.* **2015**, *6*, 7410−7417.
(42) Wang, G.; Leus, K.; Jena, H. S.; Krishnaraj, C.; Zhao, S.; Depauw, H.; Tahir, N.; Liu, Y.-Y.; Van Der Voort, P. A fluorine-containing hydrophobic covalent triazine framework with excellent selective CO2 capture performance. *J. Mater. Chem. A* **2018**, *6*, 6370−6375.
(43) Ashourirad, B.; Sekizkardes, A. K.; Altarawneh, S.; El-Kaderi, H. M. Exceptional Gas Adsorption Properties by Nitrogen-Doped Porous Carbons Derived from Benzimidazole-Linked Polymers. *Chem. Mater.* **2015**, *27*, 1349−1358.
(44) Abdelmoaty, Y. H.; Tessema, T.-D.; Norouzi, N.; El-Kadri, O. M.; Turner, J. B. M.; El-Kaderi, H. M. Effective Approach for Increasing the Heteroatom Doping Levels of Porous Carbons for Superior CO2 Capture and Separation Performance. *ACS Appl. Mater. Interfaces* **2017**, *9*, 35802−35810.
(45) Yuan, K.; Liu, C.; Zong, L.; Yu, G.; Cheng, S.; Wang, J.; Weng, Z.; Jian, X. Promoting and Tuning Porosity of Flexible Ether-Linked Phthalazinone-Based Covalent Triazine Frameworks Utilizing Substitution Effect for Effective CO2 Capture. *ACS Appl. Mater. Interfaces* **2017**, *9*, 13201−13212.
(46) Wang, K.; Tang, Y.; Jiang, Q.; Lan, Y.; Huang, H.; Liu, D.; Zhong, C. A thiophene-containing covalent triazine-based framework with ultramicropore for CO 2 capture. *J. Energy Chem.* **2017**, *26*, 902−908.
(47) Sing, K. S. W. Reporting physisorption data for gas/solid systems with special reference to the determination of surface area and porosity (Recommendations 1984). *Pure Appl. Chem.* **1985**, *57*, 603−619.
(48) Park, K.; Lee, K.; Kim, H.; Ganesan, V.; Cho, K.; Jeong, S. K.; Yoon, S. Preparation of covalent triazine frameworks with imidazolium cations embedded in basic sites and their application for CO2 capture. *J. Mater. Chem. A* **2017**, *5*, 8576−8582.
(49) Zhao, Y.; Yao, K. X.; Teng, B.; Zhang, T.; Han, Y. A perfluorinated covalent triazine-based framework for highly selective and water-tolerant CO2 capture. *Energy Environ. Sci.* **2013**, *6*, 3684−3692.
(50) Hug, S.; Mesch, M. B.; Oh, H.; Popp, N.; Hirscher, M.; Senker, J.; Lotsch, B. V. A fluorene based covalent triazine framework with high CO2and H2capture and storage capacities. *J. Mater. Chem. A* **2014**, *2*, 5928−5936.
(51) Tao, L.; Niu, F.; Liu, J.; Wang, T.; Wang, Q. Troger's base functionalized covalent triazine frameworks for CO2 capture. *RSC Adv.* **2016**, *6*, 94365−94372.

DOI: 10.1021/acsami.8b08625
ACS Appl. Mater. Interfaces 2018, 10, 26678−26686

(52) Wang, G.; Leus, K.; Zhao, S.; Van Der Voort, P. Newly Designed Covalent Triazine Framework Based on Novel N-Heteroaromatic Building Blocks for Efficient CO2 and H2 Capture and Storage. *ACS Appl. Mater. Interfaces* **2018**, *10*, 1244−1249.
(53) Saleh, M.; Lee, H. M.; Kemp, K. C.; Kim, K. S. Highly Stable CO2/N2 and CO2/CH4 Selectivity in Hyper-Cross-Linked Heterocyclic Porous Polymers. *ACS Appl. Mater. Interfaces* **2014**, *6*, 7325−7333.
(54) Ben, T.; Pei, C.; Zhang, D.; Xu, J.; Deng, F.; Jing, X.; Qiu, S. Gas Storage in Porous Aromatic Frameworks (PAFs). *Energy Environ. Sci.* **2011**, *4*, 3991−3999.
(55) Himeno, S.; Komatsu, T.; Fujita, S. High-Pressure Adsorption Equilibria of Methane and Carbon Dioxide on Several Activated Carbons. *J. Chem. Eng. Data* **2005**, *50*, 369−376.
(56) Song, W.-C.; Xu, X.-K.; Chen, Q.; Zhuang, Z.-Z.; Bu, X.-H. Nitrogen-Rich Diaminotriazine-Based Porous Organic Polymers for Small Gas Storage and Selective Uptake. *Polym. Chem.* **2013**, *4*, 4690−4696.
(57) Ma, H.; Ren, H.; Meng, S.; Sun, F.; Zhu, G. Novel Porphyrinic Porous Organic Frameworks for High Performance Separation of Small Hydrocarbons. *Sci. Rep.* **2013**, *3*, 2611.
(58) Gao, S.; Morris, C. G.; Lu, Z.; Yan, Y.; Godfrey, H. G. W.; Murray, C.; Tang, C. C.; Thomas, K. M.; Yang, S.; Schröder, M. Selective Hysteretic Sorption of Light Hydrocarbons in a Flexible Metal-Organic Framework Material. *Chem. Mater.* **2016**, *28*, 2331−2340.
(59) Zhou, Y.; Liu, B.; Sun, X.; Li, J.; Li, G.; Huo, Q.; Liu, Y. Self-assembly of Homochiral Porous Supramolecular Organic Frameworks with Significant CO2 Capture and CO2/N2 Selectivity. *Cryst. Growth Des.* **2017**, *17*, 6653−6659.
(60) Sekizkardes, A. K.; İslamoğlu, T.; Kahveci, Z.; El-Kaderi, H. M. Application of pyrene-derived benzimidazole-linked polymers to CO2 separation under pressure and vacuum swing adsorption settings. *J. Mater. Chem. A* **2014**, *2*, 12492−12500.
(61) Popp, N.; Homburg, T.; Stock, N.; Senker, J. Porous Imine-Based Networks with Protonated Imine Linkages for Carbon Dioxide Separation from Mixtures with Nitrogen and Methane. *J. Mater. Chem. A* **2015**, *3*, 18492−18504.
(62) Wang, K.; Huang, H.; Liu, D.; Wang, C.; Li, J.; Zhong, C. Covalent Triazine-Based Frameworks with Ultramicropores and High Nitrogen Contents for Highly Selective CO2 Capture. *Environ. Sci. Technol.* **2016**, *50*, 4869−4876.
(63) Arab, P.; Rabbani, M. G.; Sekizkardes, A. K.; İslamoğlu, T.; El-Kaderi, H. M. Copper(I)-Catalyzed Synthesis of Nanoporous Azo-Linked Polymers: Impact of Textural Properties on Gas Storage and Selective Carbon Dioxide Capture. *Chem. Mater.* **2014**, *26*, 1385−1392.
(64) Wang, J.; Krishna, R.; Yang, T.; Deng, S. Nitrogen-Rich Microporous Carbons for Highly Selective Separation of Light Hydrocarbons. *J. Mater. Chem. A* **2016**, *4*, 13957−13966.
(65) He, Y.; Zhang, Z.; Xiang, S.; Fronczek, F. R.; Krishna, R.; Chen, B. A Robust Doubly Interpenetrated Metal-Organic Framework Constructed from A Novel Aromatic Tricarboxylate for Highly Selective Separation of Small Hydrocarbons. *Chem. Commun.* **2012**, *48*, 6493−6495.
(66) Han, G.; Wang, K.; Peng, Y.; Zhang, Y.; Huang, H.; Zhong, C. Enhancing Higher Hydrocarbons Capture for Natural Gas Upgrading by Tuning van der Waals Interactions in fcu-Type Zr-MOFs. *Ind. Eng. Chem. Res.* **2017**, *56*, 14633−14641.
(67) Krishna, R. The Maxwell-Stefan Description of Mixture Diffusion in Nanoporous Crystalline Materials. *Microporous Mesoporous Mater.* **2014**, *185*, 30−50.
(68) Krishna, R. Methodologies for evaluation of metal-organic frameworks in separation applications. *RSC Adv.* **2015**, *5*, 52269−52295.
(69) Krishna, R. Screening Metal-Organic Frameworks for Mixture Separations in Fixed-Bed Adsorbers using A Combined Selectivity/Capacity Metric. *RSC Adv.* **2017**, *7*, 35724−35737.
(70) Krishna, R. Methodologies for Screening and Selection of Crystalline Microporous Materials in Mixture Separations. *Sep. Purif. Technol.* **2018**, *194*, 281−300.

DOI: 10.1021/acsami.8b08625
ACS Appl. Mater. Interfaces 2018, 10, 26678−26686

Supporting Information

Enhancing Gas Sorption and Separation Performance via Bisbenzimidazole Functionalization of Highly Porous Covalent Triazine Frameworks

Jianfeng Du,[†] Yuchuan Liu,[†] Rajamani Krishna[‡] Yue Yu,[†] Yuanzheng Cui,[†] Shun Wang,[†] Yunling Liu,[†] Xiaowei Song[†,] and Zhiqiang Liang[†,]**

[†] State Key Lab of Inorganic Synthesis and Preparative Chemistry, Jilin University, Changchun, 130012, P. R. China.

[‡] Van‘t Hoff Institute for Molecular Sciences, University of Amsterdam, Science Park 904, 1098 XH Amsterdam, The Netherlands

E-mail: liangzq@jlu.edu.cn; xiaoweisong@jlu.edu.cn

Materials and methods. All chemicals were purchased from commercial sources and used without further purification. **BCBIB** was synthesized in our laboratory listed in Figure S1 (ESI). Fourier transform infrared (FT-IR) spectra were collected on a Bruker IFS-66-V/S FT-IR spectrometer in the region of 400−4000 cm^{-1}. ^{1}H NMR spectra were recorded on a Varian Mercury spectrometer operating at frequency of 300 MHz. The solid state ^{13}C CP/MAS NMR spectra were recorded on a Bruker AVANCE III 400 MHz NMR spectrometer. Mass spectra were recorded on the Bruker Agilent1290 MicrOTOF Q II. Powder wide-angle X-ray diffraction (PXRD) was carried out on a Rigaku D/max-2500 X-ray diffractometer using Cu Kα radiation, operated at 40 kV and 200 mA with the 2θ ranged from 4 to 70° and a scan speed of 6° min^{-1}. Thermal gravimetric analyses (TGA) were carried out on a TGA Q500 thermogravimetric analyzer in nitrogen at a heating rate of 10 °C min^{-1}. Inductively coupled plasma (ICP) analysis was performed on a PerkinElmer Optima 3300DV spectrometer. Elemental analyses (C, H, and N) were performed with a Vario MICRO (Elementar, Germany). Scanning electron microscopy (SEM) images were recorded on a JSM-6700 M scanning electron microscope operating at 10 kV. Transmission electron microscopy (TEM) images were taken on a TECNAI F20 with an acceleration voltage of 200 kV. The Micromeritics ASAP 2020 instrument was used to evaluate the adsorption properties of N_2, CO_2 with the samples degassed at 120 °C for 12 h before testing under high vacuum. The CH_4, C_2H_6, and C_3H_8 adsorption isotherms were performed using with a Micromeritics ASAP 2020 instrument at 273 and 298 K.

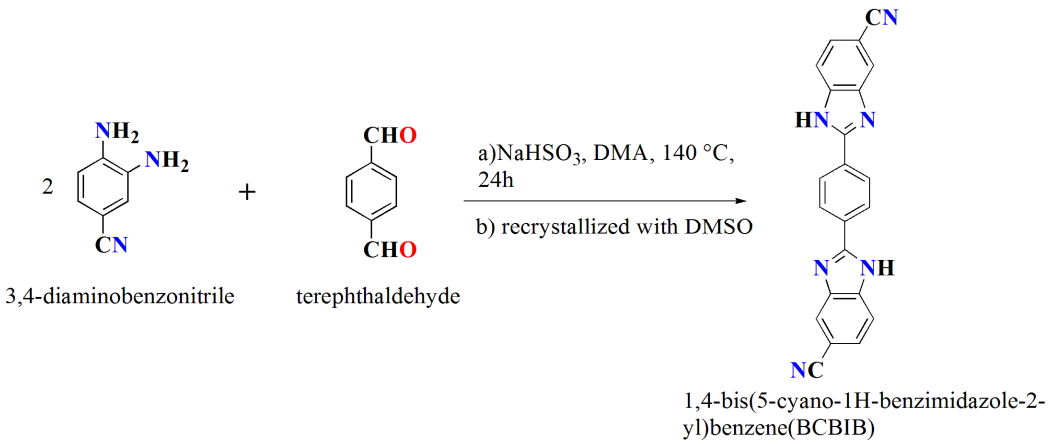

Figure S1. Synthetic scheme of **BCBIB**.

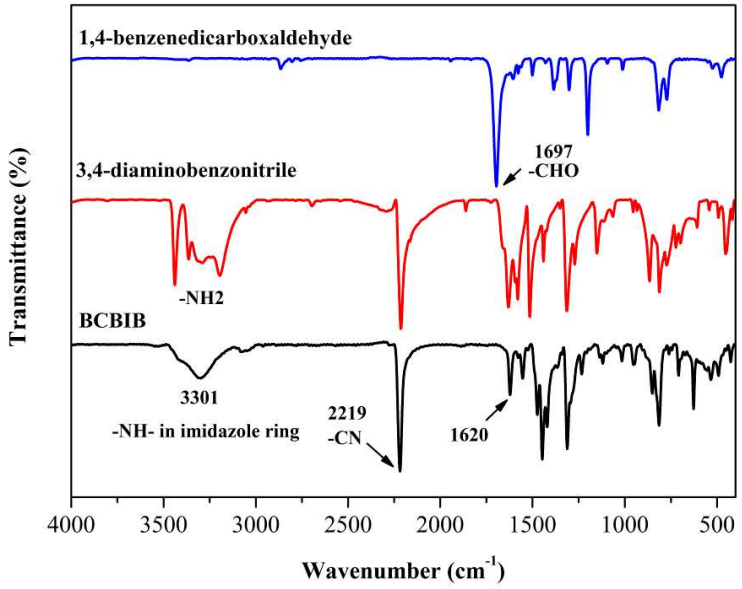

Figure S2. FT-IR spectra of **BCBIB** and corresponding reactants (KBr pellets).

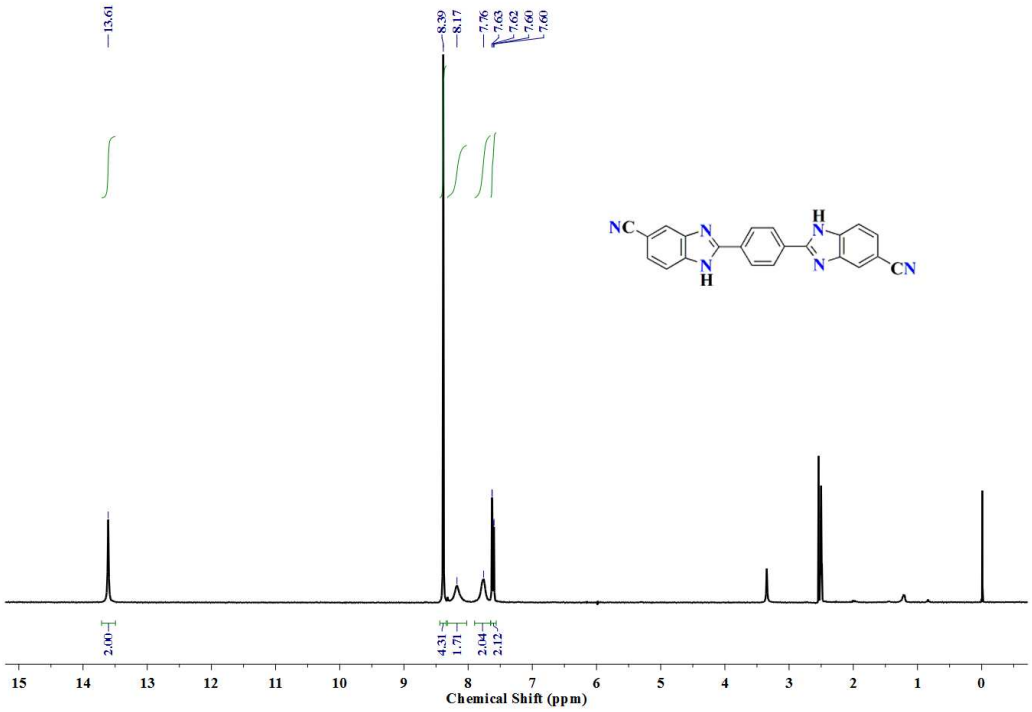

Figure S3. ^{1}H-NMR spectrum of **BCBIB**.

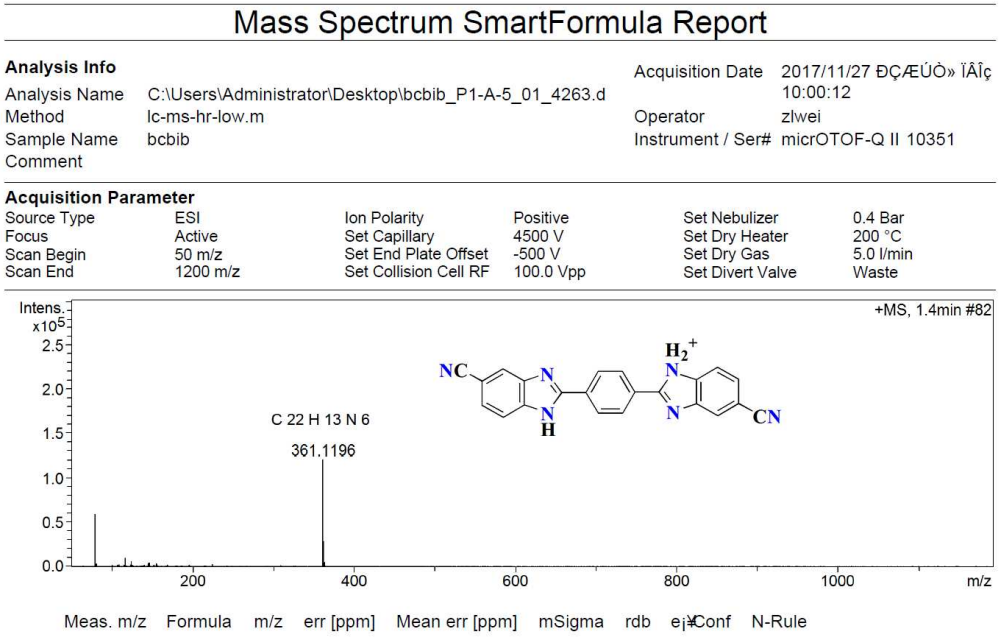

Figure S4. HRMS spectrum of **BCBIB.**

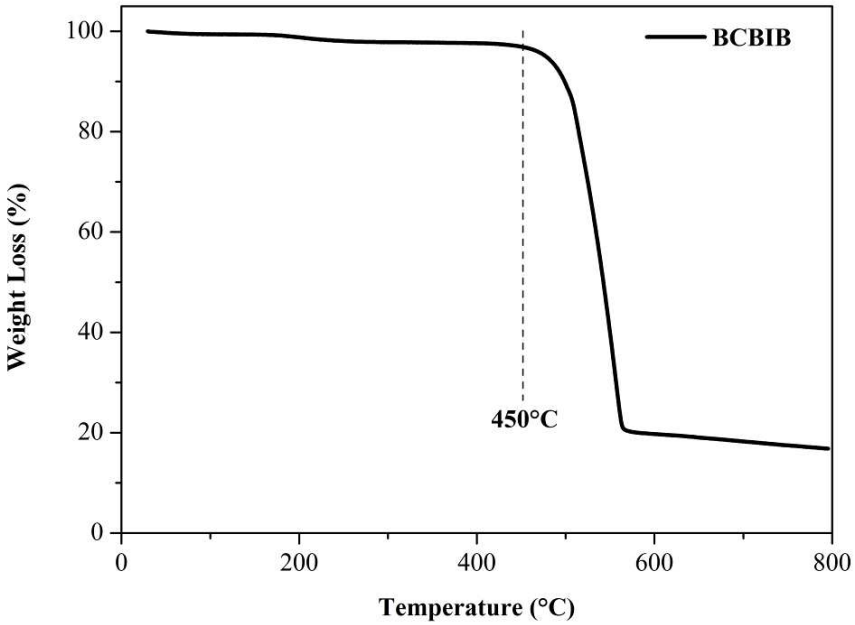

Figure S5. TGA curve of **BCBIB** under N_2 atmosphere in the range of 30 °C to 800 °C at a heating rate of 10 °C min^{-1}.

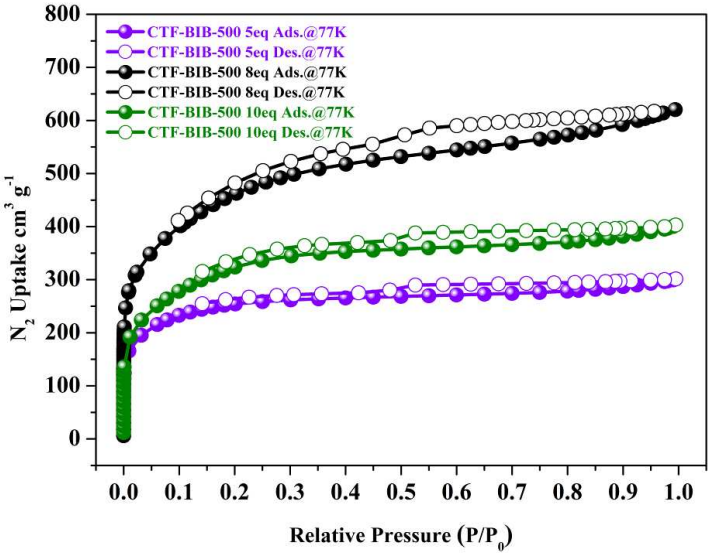

Figure S6. N_2 adsorption/desorption isotherms of **CTF-BIB-500** synthesized by using 5, 8 and 10 equivalent $ZnCl_2$, filled and empty symbols denoting adsorption and desorption, respectively. The addition of 8 eq. $ZnCl_2$ facilitates higher surface areas.

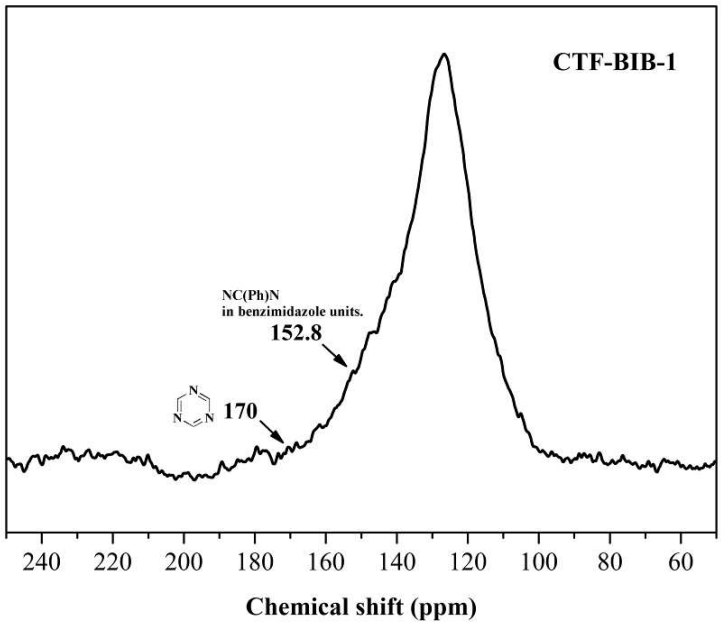

Figure S7. ^{13}C CP-MAS solid state NMR of **CTF-BIB-1**.

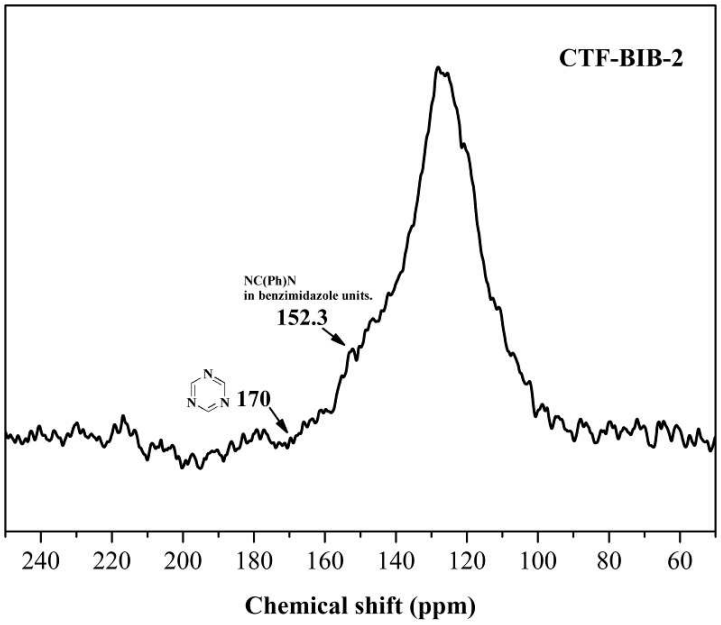

Figure S8. ^{13}C CP-MAS solid state NMR of **CTF-BIB-2**.

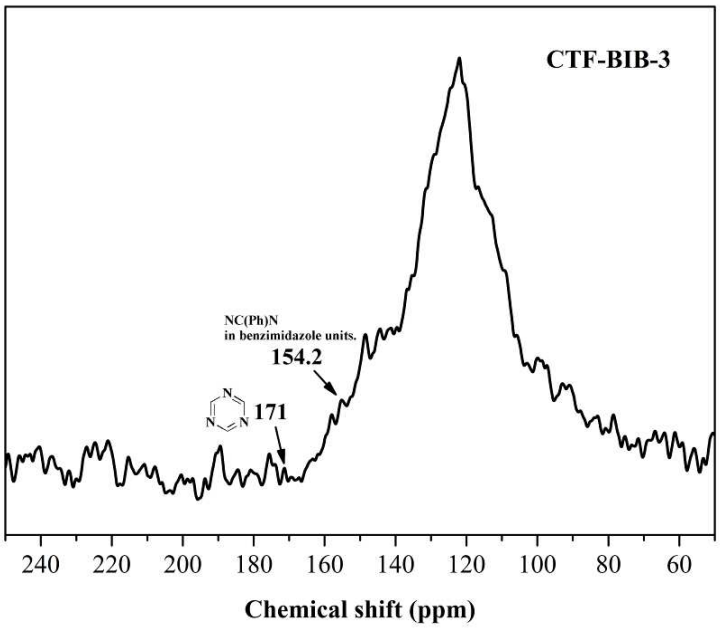

Figure S9. ^{13}C CP-MAS solid state NMR of **CTF-BIB-3**.

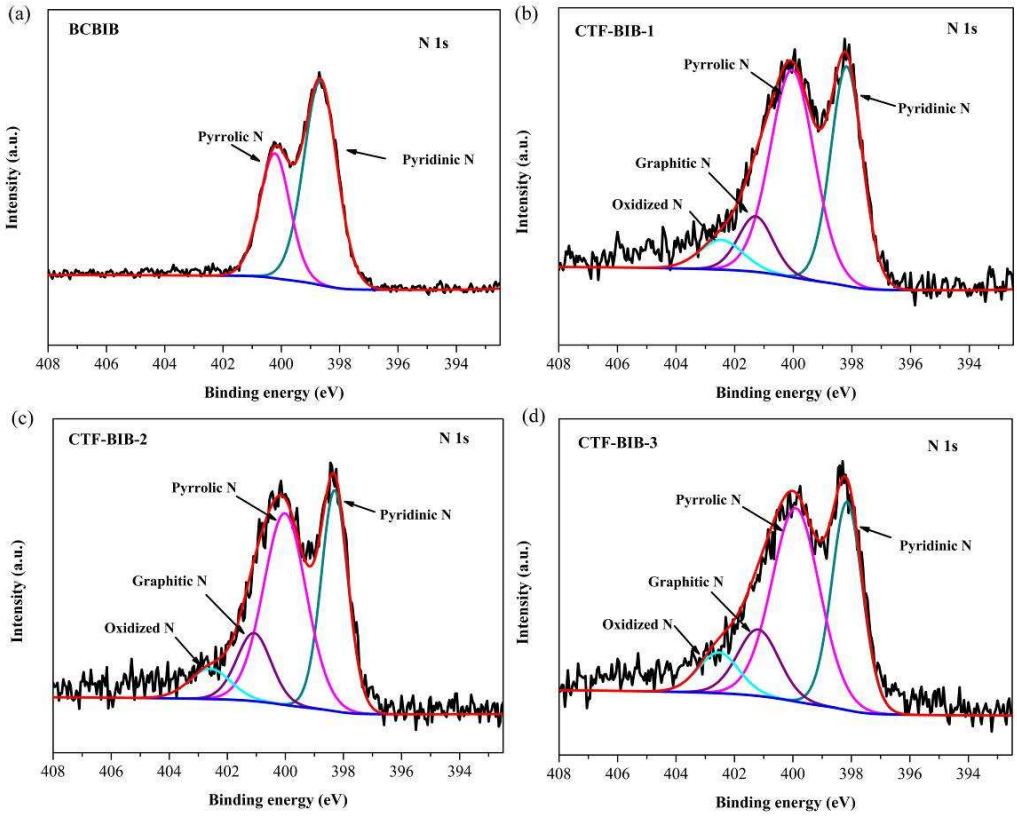

Figure S10. high-resolution signal of N 1s of **BCBIB** (a), **CTF-BIB-1** (b), **CTF-BIB-2** (c), and **CTF-BIB-3** (d).

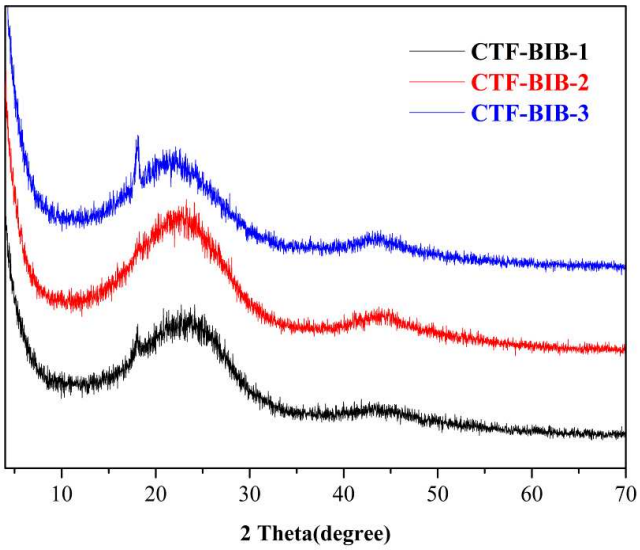

Figure S11. Powder X-ray diffraction (PXRD) patterns of **CTF-BIB-1**, **CTF-BIB-2**, **CTF-BIB-3**.

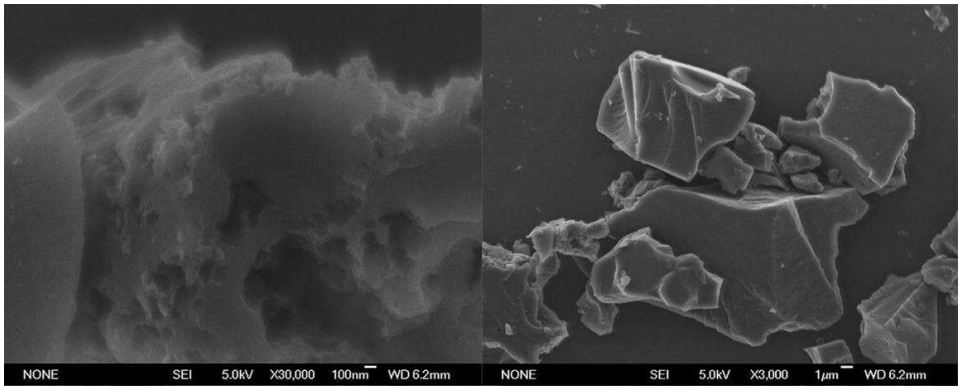

Figure S12. SEM pictures of **CTF-BIB-1** (a, b).

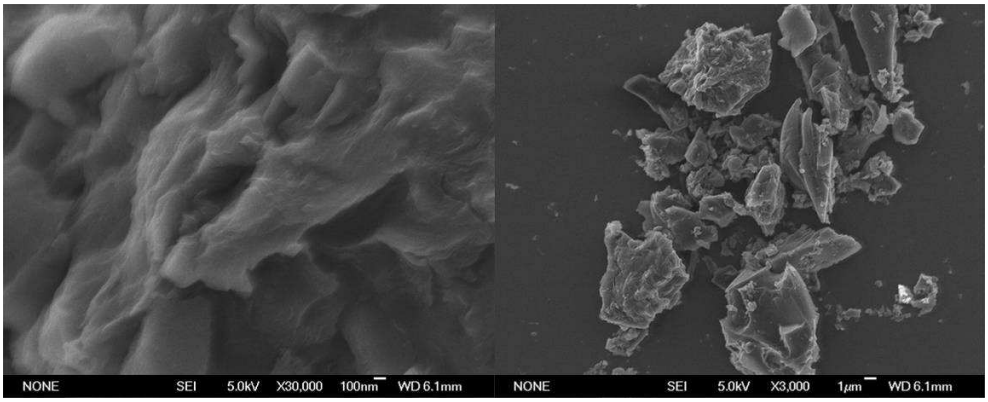

Figure S13. SEM pictures of **CTF-BIB-2** (a, b).

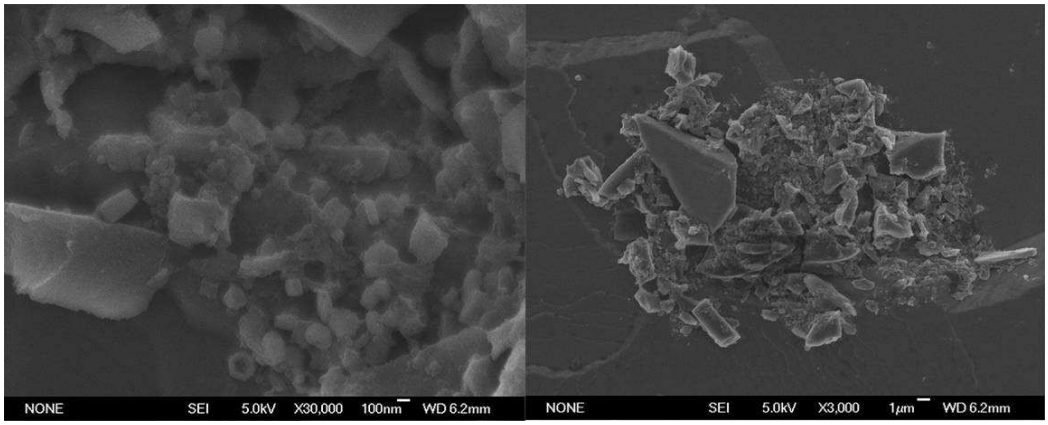

Figure S14. SEM pictures of **CTF-BIB-3** (a, b).

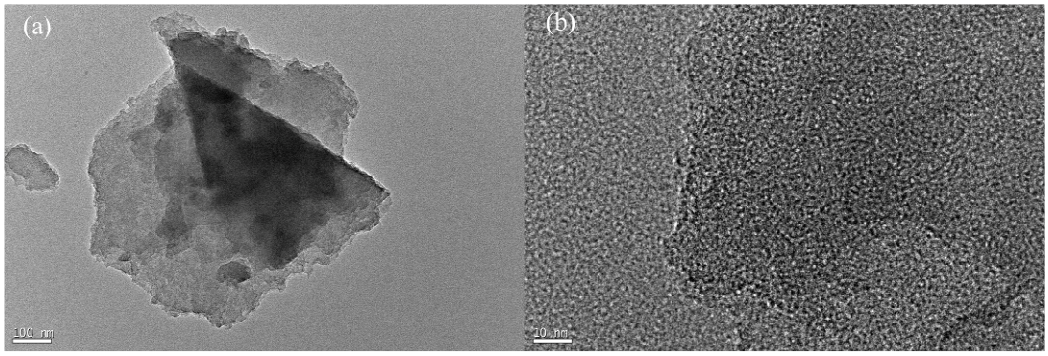

Figure S15. TEM pictures of **CTF-BIB-1** (a, b).

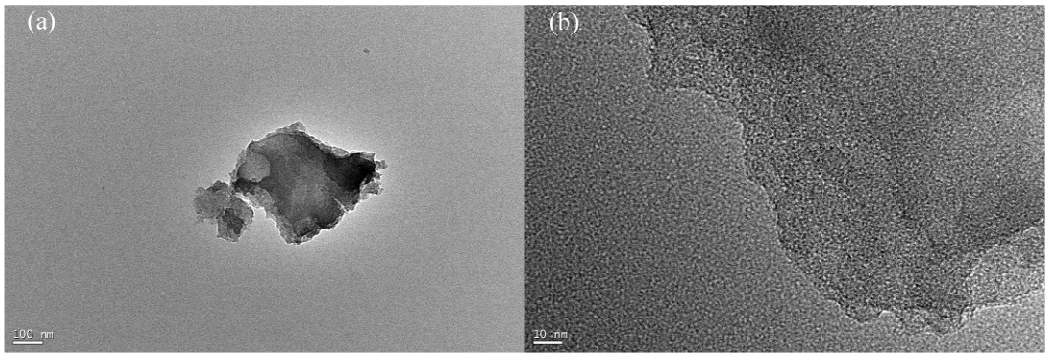

Figure S16. TEM pictures of **CTF-BIB-2** (a, b).

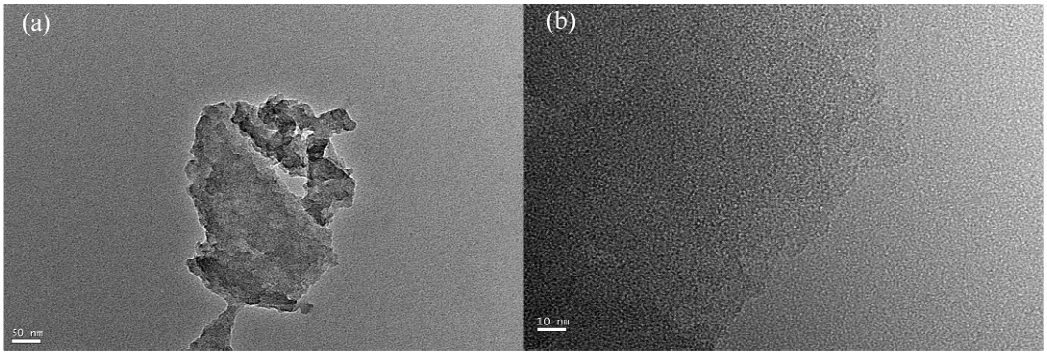

Figure S17. TEM pictures of **CTF-IB-3** (a, b).

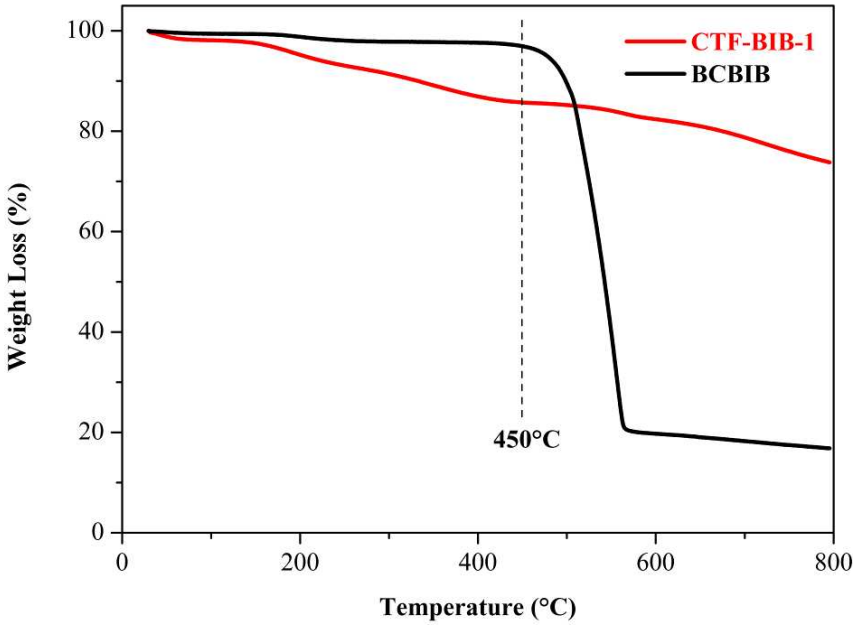

Figure S18. TGA curve of **CTF-BIB-1** under N_2 atmosphere in the range of 30 °C to 800 °C at a heating rate of 10 °C min^{-1}.

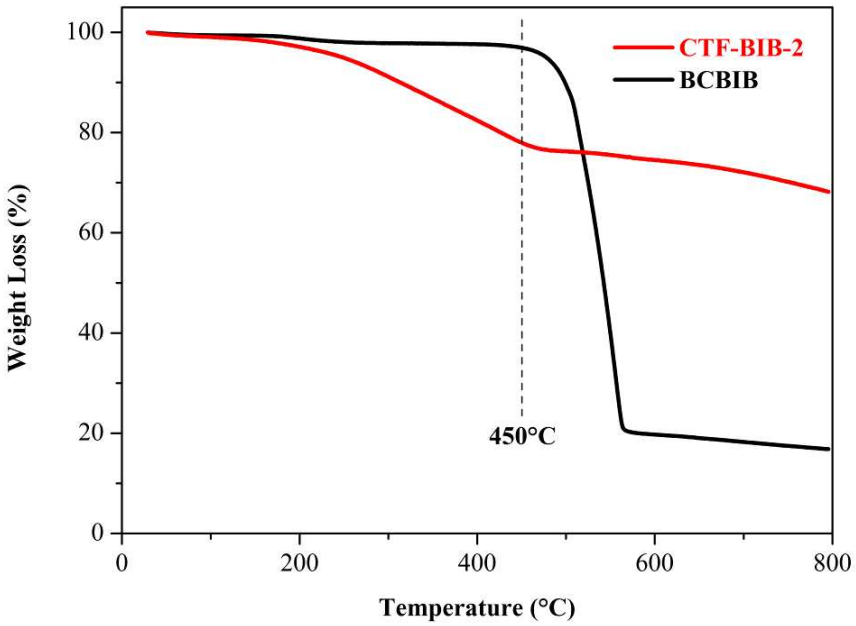

Figure S19. TGA curve of **CTF-BIB-2** under N_2 atmosphere in the range of 30 °C to 800 °C at a heating rate of 10 °C min^{-1}.

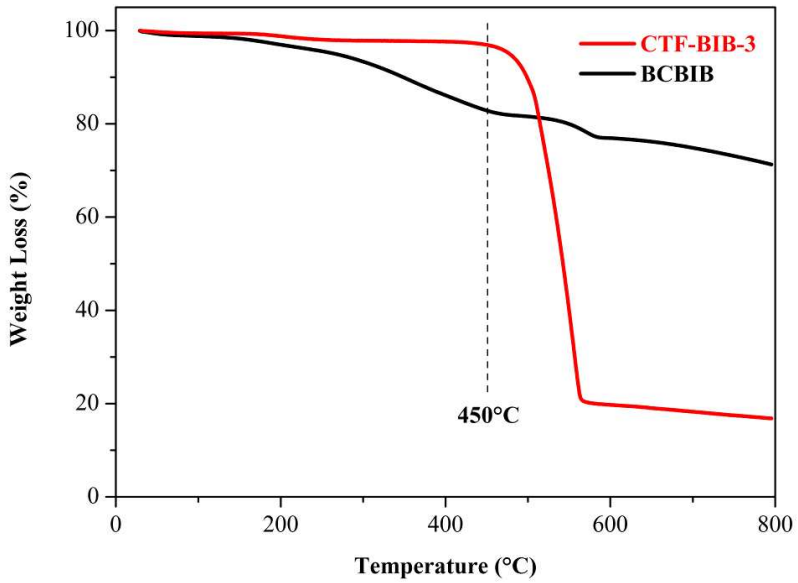

Figure S20. TGA curve of **CTF-BIB-3** under N_2 atmosphere in the range of 30 °C to 800 °C at a heating rate of 10 °C min^{-1}.

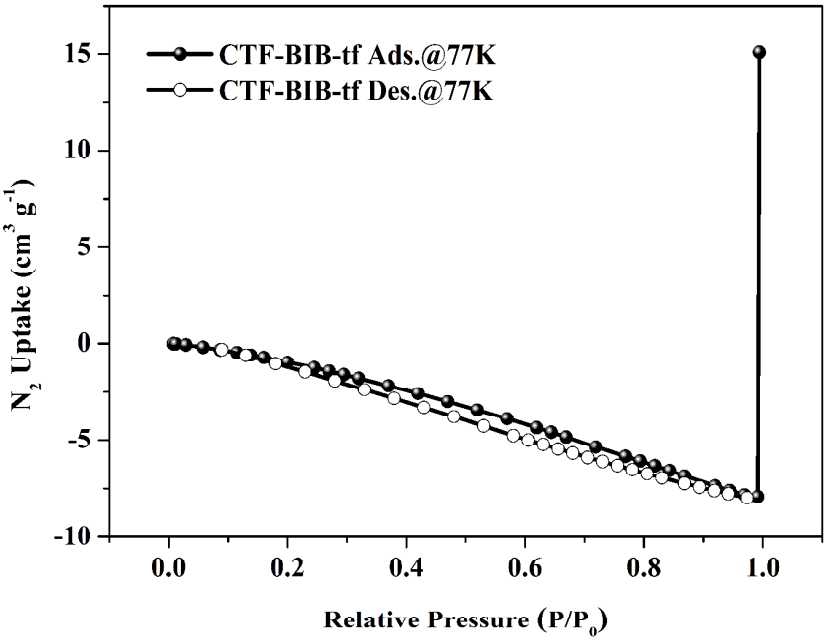

Figure S21. N_2 adsorption/desorption isotherms of **CTF-BIB-tf.**

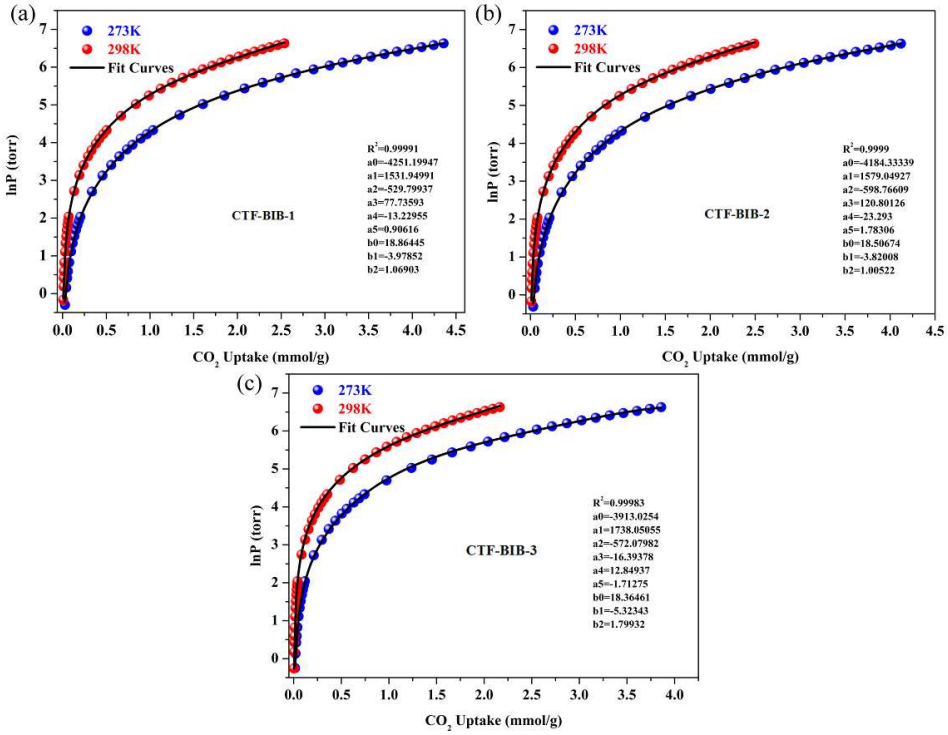

Figure S22. Q_{st} of CO_2 for **CTF-BIB-1**, **CTF-BIB-2** and **CTF-BIB-3**. (a, b, c) nonlinear curves fitting of CO_2.

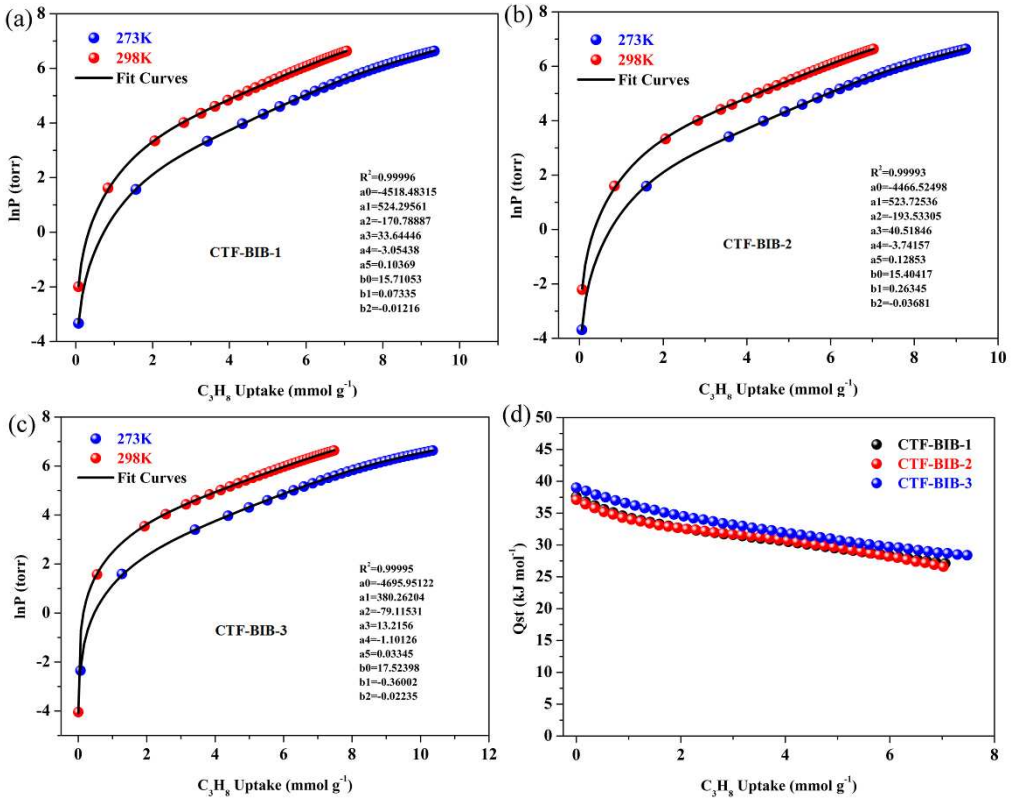

Figure S23. Q_{st} of C_3H_8 for **CTF-BIB-1**, **CTF-BIB-2** and **CTF-BIB-3**. (a-c) nonlinear curves fitting of C_3H_8; (d) calculated with virial method.

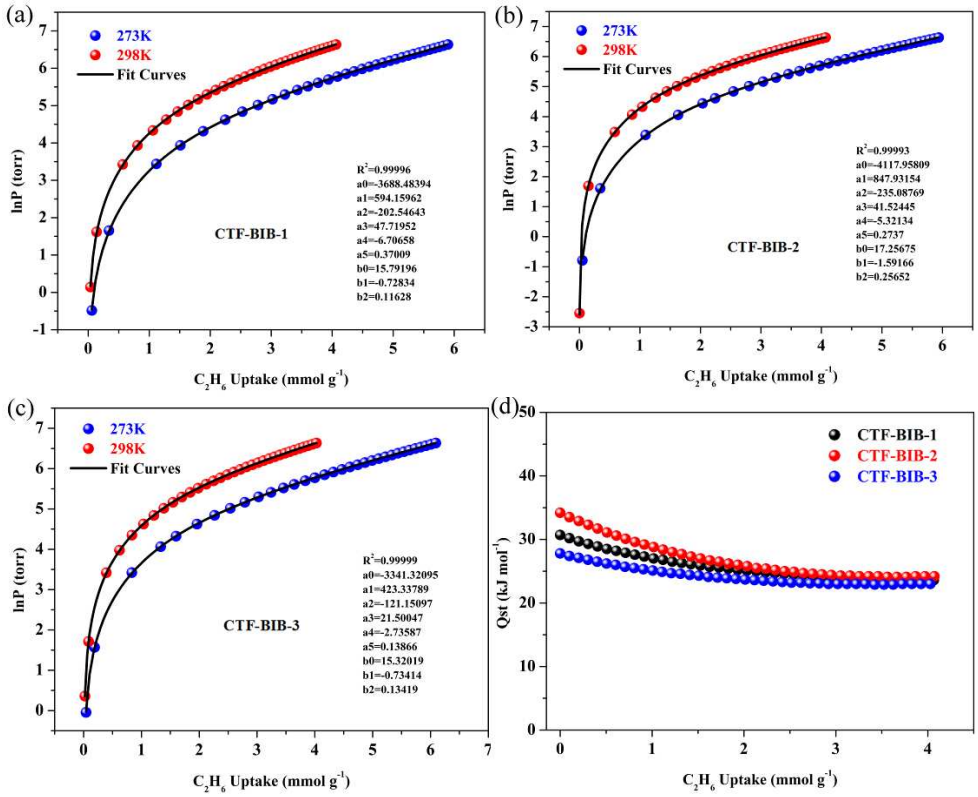

Figure S24. Q_{st} of C_2H_6 for **CTF-BIB-1**, **CTF-BIB-2** and **CTF-BIB-3**. (a-c) nonlinear curves fitting of C_3H_8; (d) calculated with virial method.

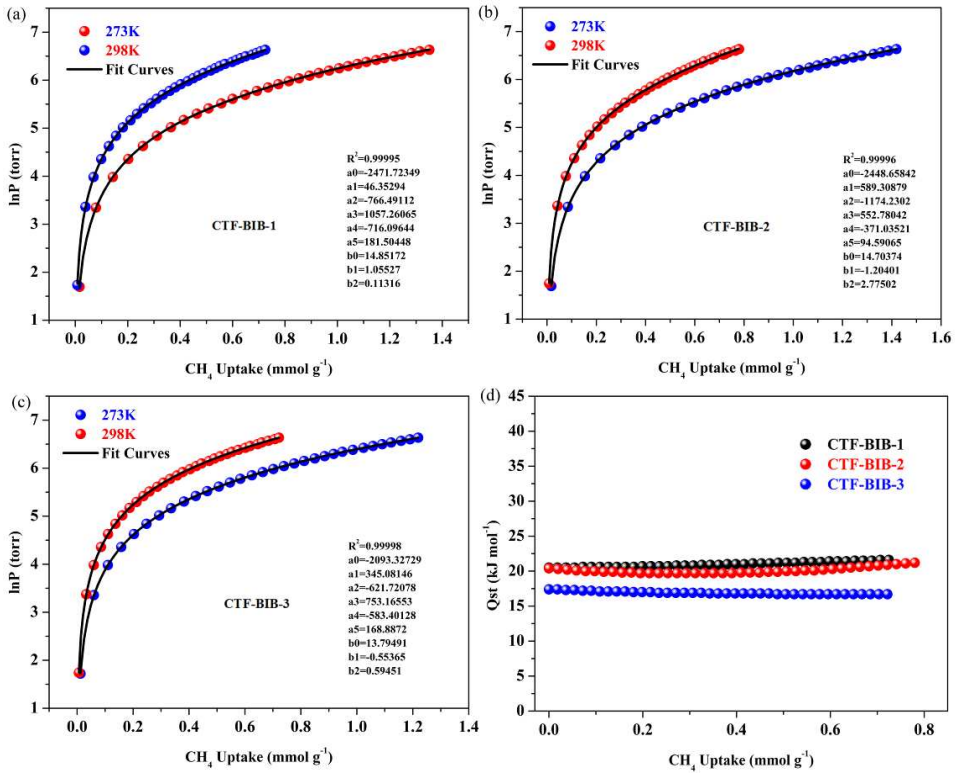

Figure S25. Q_{st} of CH_4 for **CTF-BIB-1**, **CTF-BIB-2** and **CTF-BIB-3**. (a-c) nonlinear curves fitting of C_3H_8; (d) calculated with virial method.

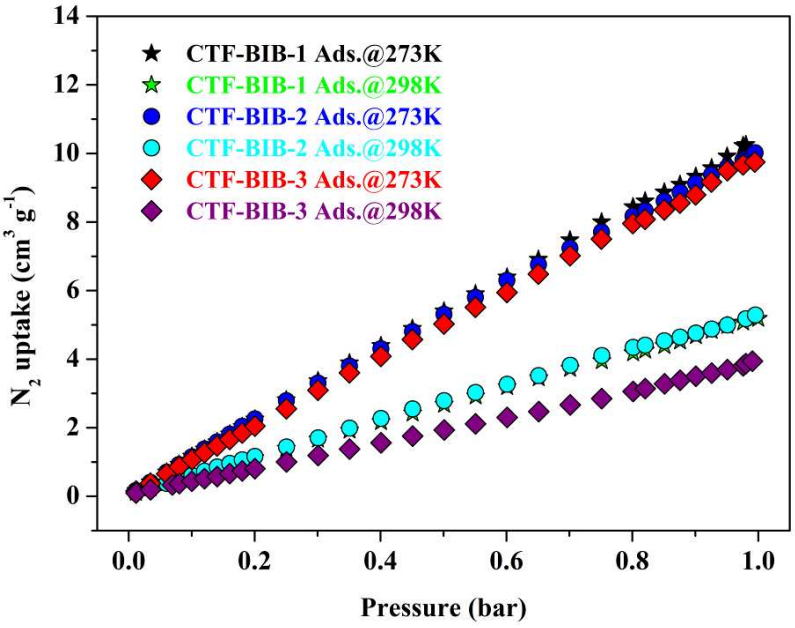

Figure S26. N_2 gas sorption isotherms for **CTF-BIB-1**, **CTF-BIB-2**, and **CTF-BIB-3** at 273 and 298 K under 1 bar

Prediction of adsorption of binary mixture by IAST theory

The measured experimental data is excess loadings (q^{ex}) of the pure components N_2, CO_2, CH_4, C_2H_6 and C_3H_8 for **CTF-BIB-1, CTF-BIB-2** and **CTF-BIB-3**, which should be converted to absolute loadings (q) firstly.

$$q = q^{ex} + \frac{pV_{pore}}{ZRT}$$

Here Z is the compressibility factor. The Peng-Robinson equation was used to estimate the value of compressibility factor to obtain the absolute loading, while the measure pore volume is also necessary.

The dual-site Langmuir-Freundlich equation[1] is used for fitting the isotherm data at 298 K.

$$q = q_{m1} \times \frac{b_1 \times p^{1/n_1}}{1 + b_1 \times p^{1/n_1}} + q_{m2} \times \frac{b_2 \times p^{1/n_2}}{1 + b_2 \times p^{1/n_2}}$$

Here p is the pressure of the bulk gas at equilibrium with the adsorbed phase (kPa), q is the adsorbed amount per mass of adsorbent (mol kg^{-1}), q_{m1} and q_{m2} are the saturation capacities of sites 1 and 2 (mol kg^{-1}), b_1 and b_2 are the affinity coefficients of sites 1 and 2 (1/kPa), n_1 and n_2 are the deviations from an ideal homogeneous surface.

The selectivity of preferential adsorption of component 1 over component 2 in a mixture containing 1 and 2, perhaps in the presence of other components too, can be formally defined as

$$S = \frac{q_1/q_2}{p_1/p_2}$$

q_1 and q_2 are the absolute component loadings of the adsorbed phase in the mixture.

These component loadings are also termed the uptake capacities. We calculate the values of q1 and q2 using the Ideal Adsorbed Solution Theory (IAST)[2] of Myers and Prausnitz.

Table S1 Porosity data of **CTF-BIBs** synthesized with different $ZnCl_2$ equivalent at 500 °C

Molar ratio of **BCBIB**/$ZnCl_2$	S_{BET}[a] ($m^2\ g^{-1}$)	V_{mic}[b] ($cm^3\ g^{-1}$)	V_{tot}[c] ($cm^3\ g^{-1}$)	V_{micro}/V_{tot}
1:5	865	0.20	0.47	0.43
1:8	1636	0.63	0.96	0.66
1:10	1141	0.11	0.62	0.18

[a] S_{BET} is the BET specific surface area. [b] V_{micro} is the pore volume determined by N_2 adsorption isotherm using t-plot method. [c] V_{tot} is the total pore volume determined by using the adsorption branch of N_2 isotherm at $P/P_o = 0.99$.

Table S2 Elemental Analysis of **CTF-BIBs**

CTF-BIBs	C (%)	H (%)	N (%)	N/C Molar Ratio (%)
CTF-BIB-1	73.35	3.13	12.96	15.7
CTF-BIB-2	74.76	3.069	10.59	12.1
CTF-BIB-3	77.50	3.779	10.41	11.5
Calc. $C_{22}H_{12}N_6$	73.32	3.36	23.32	27.3

Table S3 The refined parameters for the Dual-site Langmuir-Freundlich equations fit for the pure isotherms of N_2, CO_2, CH_4, C_2H_6 and C_3H_8 for **CTF-BIB-1**, **CTF-BIB-2** and **CTF-BIB-3** at 298 K.

CTF-BIBs	Gas	q_{m1}	b_1	$1/n_1$	q_{m2}	b_2	$1/_{n2}$	R^2
	N_2	0.02175	0.09066	0.43229	5.40738	3.28372E-4	1.01124	0.99984
	CO_2	0.38055	0.0896	1.01593	9.77842	0.0039	0.92788	0.99999
CTF-BIB-1	CH_4	3.13064	0.00149	1.05727	0.31454	0.01717	0.92191	0.99991
	C_2H_6	0.52344	0.15112	0.92971	10.12339	0.01202	0.82326	0.99999
	C_3H_8	7.16567	4.10859E-5	1.5811	9.94893	0.11507	0.61526	0.99999
	N_2	1.96171	6.19585E-4	1.06606	0.17162	0.00964	0.7534	0.99966
	CO_2	0.60237	0.07796	0.93403	12.88239	0.00257	0.91677	0.99999
CTF-BIB-2	CH_4	3.90236	0.00264	0.94569	0.01669	0.00368	1.73561	0.99988
	C_2H_6	9.10187	0.00849	0.90521	0.89835	0.14807	0.82142	0.99999
	C_3H_8	7.92959	2.89646E-4	1.22644	9.01312	0.12832	0.63411	0.99998
	N_2	0.91669	1.21459E-7	2.66347	68.36308	3.19397E-5	0.84018	0.99977
	CO_2	9.52149	0.000247	0.99747	0.26534	0.06558	1.07857	0.99999
CTF-BIB-3	CH_4	4.07905	0.00178	1.02022	0.00325	0.37776	1.71779	0.99992
	C_2H_6	1.02966	0.07836	0.90496	8.31068	0.00463	1.0537	0.99999
	C_3H_8	9.97364	1.17751E-4	1.42645	9.16197	0.08575	0.74195	0.99999

Transient breakthrough of mixtures in fixed bed adsorbers

The performance of industrial fixed bed adsorbers is dictated by a combination of adsorption selectivity and uptake capacity. Transient breakthrough simulations were carried out for equimolar $CO_2/C_3H_8/C_2H_6/CH_4$ mixtures operating at a total pressure of 100 kPa and 298 K, using the methodology described in earlier publications. For the breakthrough simulations, the following parameter values were used: length of packed bed, L = 0.3 m; voidage of packed bed, ε= 0.4; superficial gas velocity at inlet, u = 0.04 m/s. The transient breakthrough simulation results are presented in terms of a *dimensionless* time as the x-axis, τ, defined by dividing the actual time, t, by the characteristic time, $\frac{L\varepsilon}{u}$. The y-axis is the dimensionless gas concentration at the outlet of the fixed bed adsorber, c_i/c_{i0}.

Notation

b	Langmuir-Freundlich constant, $Pa^{-\nu}$
c_i	molar concentration of species i in the gas phase, mol m^{-3}
c_{i0}	molar concentration of species i at inlet to adsorber, mol m^{-3}
p_i	partial pressure of species i in mixture, Pa
q	component molar loading of species i, mol kg^{-1}
q_{sat}	saturation loading, mol kg^{-1}
L	length of packed bed adsorber, m
R	gas constant, 8.314 J mol^{-1} K^{-1}
t	time, s

T absolute temperature, K

u superficial gas velocity in packed bed, m s^{-1}

Greek letters

ε voidage of packed bed, dimensionless

v Freundlich exponent, dimensionless

τ time, dimensionless

ρ framework density, kg m^{-3}

Reference

1. Ruthven, D.M. Principles of Adsorption and Adsorption Processes; Wiley: New York, 1984.

2. Myers, A. L.; Prausnitz, J. M. Thermodynamics of mixed-gas adsorption. *AIChE. J.* **1965**, *11*, 121-127.